Am J Transl Res 2026;18(3):1826-1845
www.ajtr.org /ISSN:1943-8141/AJTR0171601

Original Article

ECE1c promotes glioblastoma invasion via the ROCK2-MYH10 axis and interaction with ACTB

Liangliang Wang[1,2,3], Feihu Zhao[1,2], Yanfei Sun[1,3], Jilong Liu[1,3], Jiazheng Wang[1,3], Jian Wang[1,4], Bin Huang[1,3], Xingang Li[1,3]

[1]Department of Neurosurgery, Qilu Hospital, Cheeloo College of Medicine and Institute of Brain and Brain-Inspired Science, Shandong University, Jinan 250012, Shandong, China; [2]Department of Neurosurgery, The Second Qilu Hospital of Shandong University, Cheeloo College of Medicine, Shandong University, Jinan 250033, Shandong, China; [3]Jinan Microecological Biomedicine Shandong Laboratory and Shandong Key Laboratory of Brain Function Remodeling, Jinan 250017, Shandong, China; [4]Department of Biomedicine, University of Bergen, Jonas Lies Vei 91, 5009, Bergen, Norway

Received January 21, 2026; Accepted February 27, 2026; Epub March 15, 2026; Published March 30, 2026

Abstract: Background: Glioblastoma is the most malignant primary intracranial tumor and is characterized by rapid growth, diffuse invasion, and notable therapeutic resistance. The mesenchymal subtype of glioblastoma multiforme (GBM) is the most aggressive, but the underlying regulatory network of this phenotype has not yet been fully elucidated. Methods: Bioinformatic analysis was performed to identify the heterogeneity of ECE1 expression and its prognostic roles. Cytological experiments were conducted to evaluate the function of ECE1 in GBM cell lines. Tumor xenograft models were established to access intracranial GBM growth *in vivo*. Protein interactions and signaling mechanisms were investigated by coimmunoprecipitation, immunofluorescence, and Western blot. Results: In the present study, our analyses revealed that ECE1 is closely associated with the mesenchymal subtype, CD44 expression, and prognosis of GBM. We found that ECE1c was the most common isoform in GBM. The knockdown of ECE1 reduced both the proliferation and invasiveness of GBM cells, whereas overexpression of ECE1c promoted tumor malignancy. Mechanistic studies revealed that ECE1c activates the ROCK2 signaling pathway and interacts with ACTB, thereby modulating cytoskeletal remodeling and promoting pseudopodia formation, which together increase the invasive capacity of GBM. Conclusion: Our results indicate that ECE1c is a key regulator of GBM invasion through ROCK2 activation and interaction with ACTB. Targeting ECE1c may represent a viable therapeutic strategy for treating invasive GBM.

Keywords: Glioblastoma, ECE1, ROCK2, ACTB, invasion

Introduction

Glioblastoma multiforme (GBM) is the most aggressive and lethal primary malignant intracranial neoplasm and is characterized by widespread infiltration, rapid proliferation, and inevitable recurrence despite maximal multimodal therapy [1, 2]. The current standard Stupp procedure consists of surgery, radiation therapy, and temozolomide administration. Even if this treatment only slightly improves survival, the median overall survival time is still approximately 15 months [3-5]. The heterogeneity of GBM is among the main reasons why it is so dangerous and difficult to treat [6]. According to molecular profiling, there are three main forms of GBM: classic (CL), proneural (PN), and mesenchymal (MES) [7-9]. Of these GBM subtypes, the MES GBM has the most aggressive phenotype. It is very invasive and resistant to standard treatments, and it spreads throughout the surrounding brain parenchyma, making it impossible to remove completely through surgery and contributing to inevitable recurrence [8-10]. Characterized by a CD44-rich hallmark, these subtypes of GBM promote cell proliferation, migration, and therapeutic resistance [9]. Given the highly invasive nature and treatment-refractory behavior of MES GBM, elucidating the molecular mechanisms that drive its migra-

https://doi.org/10.62347/SQBU5335

tory and infiltrative potential is important. These findings will help us discover new therapeutic targets and improve clinical outcomes.

The endothelin (ET) signaling pathway, which includes endothelin-1 (ET-1), its receptors (ET_AR and ET_BR), and endothelin-converting enzymes (ECEs), is strongly linked to the formation of tumors [11, 12]. In the tumor microenvironment, this ET system regulates various critical activities, including cell proliferation, angiogenesis, invasion, and immune evasion [11]. ET-1, which is produced from big ET-1 by ECE1, is implicated in numerous malignancies; nevertheless, increasing amounts of data indicate that ECE1 may promote tumor progression independently of ET-1 signaling [13-16]. In GBM, pharmacological inhibition of ECE1 reduces GBM cell proliferation without affecting ET-1 concentrations, and the application of exogenous ET-1 fails to rescue the proliferation deficit [14, 17], which indicates that ECE1 may play a unique, noncanonical oncogenic role outside of its primary function in ET-1 processing. There are four isoforms of ECE1 (ECE1a-d) that result from alternative splicing and have small differences in their N-terminal sequences [12]. ECE1c has been identified as the predominant isoform in several cancers [12, 18, 19]. ECE1c enhances invasiveness in prostate, colorectal, and lung cancers [17, 18, 20]. The phosphorylation of ECE1c by casein kinase 2 (CK2) significantly increases its stability and endows it with carcinogenic potential by facilitating invasive phenotypes [21, 22]. Despite advances in elucidating the function of ECE1c, the downstream molecular mechanisms through which ECE1c drives GBM invasion remain unclear.

As a downstream effector of the Rho GTPase, Rho-associated coiled-coil containing protein kinase 2 (ROCK2) plays a crucial role in regulating actomyosin contractility, cytoskeletal reorganization, and epithelial-mesenchymal transition (EMT) [23]. The activation of ROCK2 promotes the activation of matrix metalloproteinases (MMPs) and the production of stress fibers, both of which are essential for tumor invasion and metastasis [24, 25]. Moreover, aberrant ROCK2 activation has been correlated with heightened tumor aggressiveness and metastatic potential in several malignancies, including hepatocellular carcinoma, pancreatic cancer, and oligodendrogliomas [26-28]. Nevertheless, the mechanism through which ECE1 promotes GBM invasion through ROCK2 signaling is unclear.

In addition to ROCK2 signaling, the dynamics of the actin cytoskeleton are crucial for facilitating tumor cell motility. β-actin (ACTB), a principal component of filamentous actin (F-actin), forms the structural basis of protrusive pseudopodia, such as lamellipodia and filopodia, which enable directed cellular movement and invasion [24, 29]. Additionally, dysregulation of actin polymerization and organization has been associated with increased motility and therapeutic resistance in GBM [30]. However, whether ECE1 interacts with cytoskeletal components such as ACTB to influence cellular morphology and invasion dynamics has not been determined.

This research revealed that ECE1 is a pivotal gene associated with the MES subtype of GBM and CD44 expression. We validated ECE1c as the predominant isoform in GBM cells and investigated its function in enhancing glioblastoma invasiveness. We demonstrated that suppression of ECE1 inhibited the growth, motility, and invasion of GBM, whereas overexpression of ECE1c exacerbated these malignant features. Mechanistically, we demonstrated that ECE1c facilitates GBM cell invasion through a dual mechanism: activation of the ROCK2 signaling axis and interaction with ACTB. These processes alter the cytoskeleton and enhances pseudopodia formation. Our findings reveal a previously unidentified ECE1-dependent regulatory mechanism in GBM, suggesting that targeting ECE1c may represent a feasible treatment strategy for invasive GBM.

Materials and methods

Bioinformatics analysis

The data used in this study were obtained from publicly available databases, including the Chinese Glioma Genome Atlas (CGGA: https://www.cgga.org.cn) [31], The Cancer Genome Atlas (TCGA: https://portal.gdc.cancer.gov), and the Genotype-Tissue Expression (GTEx: https://xena.ucsc.edu). Bioinformatics analyses were conducted using the GEPIA2 (http://gepia2.cancer.cn), GlioVis (http://gliovis.bioinfo.cnio.es), and STRING (https://string-db.org) [32] web platforms, as well as R software. The TCGA

or CGGA (mRNAseq_693) datasets were integrated with GTEx data following normalization and preprocessing. Differentially expressed gene (DEG) analysis was performed using the *edgeR* and *ggplot2* packages. DEGs between the mesenchymal subtype and other subtypes, or between CD44 and others, were identified using the *limma* package.

Cell culture

The cells utilized in the experiments included human glioblastoma cell lines (LN229, A172, and U87MG, acquired from the Cell Bank of the Chinese Academy of Sciences), the human embryonic kidney cell line HEK293T (sourced from the Cell Bank of the Chinese Academy of Sciences), patient-derived glioblastoma stem-like cells (GSCs; GBM#BG5, obtained from Prof. Rolf Bjerkvig), and normal human astrocytes (NHA; purchased from Lonza). HEK293T, LN229, A172 and U87MG cells were grown in Dulbecco's modified Eagle's medium (Thermo Fisher Scientific) supplemented with 10% fetal bovine serum (FBS; Thermo Fisher Scientific). BG5 cells were cultured in Neurobasal medium (Gibco, Thermo Fisher Scientific) supplemented with epidermal growth factor (EGF; 20 ng/mL, Thermo Fisher Scientific), basic fibroblast growth factor (bFGF; 10 ng/mL, Thermo Fisher Scientific), and B27 supplement (2%, Thermo Fisher Scientific). NHA cells were maintained in BulletKit astrocyte medium. All cells were cultured in a cell incubator at 37°C with 5% CO_2. The cells were periodically passaged, and cells in the logarithmic growth phase were used in subsequent experiments.

Transient transfection, lentivirus construction, and infection

GenePharma (Shanghai, China) provided small interfering RNAs (siRNAs) that targeting human ECE1 and negative control siRNAs. Transient transfection of siRNAs or plasmids was performed using Lipofectamine 3000 (Thermo Fisher Scientific) according to standard protocols. Knockdown efficiency was verified by quantitative real-time PCR (qRT-PCR) and immunoblotting at 72 hours post-transfection. HEK-293T cells were cotransfected with psPAX2, pCMV-VSV-G, and expression vectors. The viral supernatant was harvested after 48 h and clarified by filtration. Target cells were then exposed to the lentivirus for 48 h and subsequently selected in puromycin-containing medium (2 μg/mL; Thermo Fisher Scientific) for two weeks. The siRNA sequences targeting ECE1 were as follows: siCtrl: 5'-UUCUCCGAACGUGUCACG-UTT-3', siECE1-2#: 5'-GCCUGCUCAACAACUAC-AUTT-3', and siECE1-3#: 5'-GGACCAGUCCAG-UCCUCUAGU-3'.

Cell proliferation assay

The proliferation of GBM cells was assessed via an EdU incorporation assay (RiboBio). LN229, U87MG, and A172 cells were cultured in 24-well plates (2×10^4 cells per well) and transfected with ECE1-targeting siRNA for 48 hours. EdU labeling and subsequent fluorescence staining were performed in accordance with standard protocols. Fluorescence images were obtained using a Leica fluorescence microscope, and the percentage of EdU-positive cells was subsequently calculated.

Cell viability was assessed by a Cell Counting Kit-8 (CCK-8; Beyotime Biotechnology). U87MG, A172, and LN229 cells (3×10^3 cells per well) or GBM#BG5 cells (1×10^4 cells per well) were seeded into 96-well plates. At 24, 48, 72, and 96 hours post-treatment, 10 μL of CCK-8 reagent was added to each well and incubated for 30 minutes at 37°C. The absorbance was measured at 450 nm.

Cell migration assays

After transfection with siRNA for 48 h, the cells were plated in 6-well plates (5×10^5 cells per well) for the wound-healing assay. When the cells reached approximately 90% confluence, a straight scratch was created using a 200 μL pipette tip. Images of the same field were captured at 0 and 12 hour using an inverted microscope (Olympus).

Transwell migration assays were conducted using 24-well chambers with 8.0 μm pores (Corning). Cells transfected with siECE1 were plated in the upper chamber in serum-free DMEM, and the lower chamber was filled with DMEM supplemented with 30% FBS. After incubation for 24-48 hours, the non-migrated cells on the upper surface of the membrane were removed, and the migrated cells were fixed with 4% paraformaldehyde (Biosharp) and stained with crystal violet (Beyotime Biotechnology), and quantified microscopically.

Cell invasion assays

Spheroid-based invasion assays were conducted to assess invasive potential. After siRNA transfection for 48 hours, GBM spheroids were embedded in an invasion matrix (Trevigen). At 0, 24, and 48 hours, the spheroids were imaged under an inverted microscope, and the invasion distance was calculated relative to the initial spheroid diameter.

Spheroid formation and limiting dilution assay

For the spheroid formation assay, isolated single BG5 cells were plated in 96-well plates (1 cell/μl per well) and cultured for 7 days, after which the diameter of each spheroid was measured. For the limiting dilution assay, BG5 cells were seeded into 96-well plates at densities of 5, 10, 20, 40, 80, 160, 320, and 640 cells per well, with 15 replicate wells for each cell density. After 14 days of culture, wells containing at least one tumor sphere with a diameter ≥50 μm were counted. Analysis was performed using GraphPad Prism software.

Immunohistochemistry (IHC)

Tumor tissues derived from orthotopic xenografts were fixed, paraffin-embedded, and sectioned. IHC staining was carried out following established procedures. The primary antibodies used were mouse anti-ECE1 (sc-376017, 1:100, Santa Cruz Biotechnology) and rabbit anti-Ki67 (GB111499, 1:400, Servicebio). Ki67-positive nuclei were calculated based on the percentage of DAB-positive cells, and ECE1 expression levels were evaluated using semi-quantitative IHC scores combining staining intensity and positive staining area.

Coimmunoprecipitation (Co-IP)

Cells were lysed in prechilled IP lysis buffer (Thermo Fisher Scientific) containing protease inhibitors (Biotech Biotechnology). The cell lysates were centrifuged at 12,000×g for 15 min at 4°C, after which the supernatants were collected. A portion of the sample was kept as input, and the remainder was incubated with anti-ECE1, anti-ACTB, or IgG overnight at 4°C. The samples were then mixed with protein A/G magnetic beads (Thermo Fisher Scientific) and incubated at room temperature for 1 hour, after which the immune complexes were subjected to immunoblot analysis. The antibodies used included mouse anti-ECE1 (sc-376017, 1:100, Santa Cruz Biotechnology), mouse anti-ACTB (66009-1-Ig, 1:100, Proteintech), and normal mouse IgG (68860L, 1:100, Cell Signaling Technology).

Western blotting

Total protein was extracted for Western blotting using RIPA buffer supplemented with phosphatase and protease inhibitors (Beyotime Biotechnology). Protein concentrations were quantified using a BCA assay (Beyotime Biotechnology). Equal amounts of protein samples were separated by SDS-PAGE and subsequently electrotransferred onto PVDF membranes. After blocked with nonfat milk (5%, 1 h), the membranes were incubated overnight with primary antibodies at 4°C and subsequently probed with HRP-linked secondary antibodies (1:5000). Protein bands were detected with an ECL detection kit (Millipore) and captured using a chemiluminescence imaging system (Bio-Rad). Densitometric analysis was performed with ImageJ, and protein levels were normalized to β-tubulin. The primary antibodies used included anti-ECE1 (sc-376017, Santa Cruz Biotechnology), anti-β-tubulin (AC008, ABclonal), anti-ROCK2 (21645-1-AP; Proteintech), anti-N-cadherin (66219-1-Ig, Proteintech), anti-MMP2 (66366-1-Ig, Proteintech), anti-MYH10 (19673-1-AP, Proteintech), and anti-Slug (C19G7, Cell Signaling Technology).

Real-time quantitative PCR

Total RNA was isolated using an RNA-Quick Purification Kit (RN001, eSUN Bio). RNA concentration and purity were determined using a NanoDrop One (Thermo Fisher Scientific). Subsequently, 1 μg of RNA was subjected to genomic DNA removal, and the PrimeScript RT Reagent Kit (Takara) was used for reverse transcription into cDNA. Quantitative reverse transcription polymerase chain reaction (qRT-PCR) was performed using a Hieff qPCR SYBR Kit (Yeasen Biotechnology) on a LightCycler 96 system (Roche). Tubulin was used as the internal control, and the $2^{-\Delta\Delta Ct}$ method was employed to determine relative gene expression. All reactions were conducted in triplicate. The primers used are listed in Table S1.

Mass spectrometry analysis

LN229 cells were subjected to Co-IP using IgG and anti-ECE1 antibodies. The immunoprecipitated complexes were validated by Western blotting and subsequently analyzed by liquid chromatography-mass spectrometry (HPLC-MS/MS, QLBio, China) to identify ECE1-interacting proteins.

RNA sequencing analysis

Total RNA was extracted from LN229 cells transfected with siECE1 or negative control siRNA using TRIzol reagent (Invitrogen). RNA integrity was evaluated, and the RNA libraries were sequenced on the Illumina Novaseq™ 6000 platform by LC Bio Technology Co., Ltd. (Hangzhou, China). Differentially expressed genes were analyzed using DESeq2 in R, with adjusted p values < 0.05 considered significant. Enrichment analysis for Gene Ontology (GO) and Kyoto Encyclopedia of Genes and Genomes (KEGG) pathways was conducted using the clusterProfiler package.

Immunofluorescence (IF)

For confocal imaging, 3×10^4 cells were seeded onto coverslips in 24-well plates, fixed with 4% paraformaldehyde for 15 minutes, and blocked with 5% BSA for 1 h. ECE1 labeling was performed using the FlexAble 2.0 CoraLite® Plus 488 Antibody Labeling Kit (KFA521, Proteintech) overnight at 4°C. The cells were subsequently counterstained with IF555-Phalloidin (G1249-100T, Servicebio) for 60 min, after which they were stained with DAPI using Antifade Mounting Medium (P0131-5 mL, Beyotime Biotechnology). Images were captured using a laser confocal microscope (Leica).

Xenografts

Male nude mice (4 weeks old, ~15 g) were anesthetized and implanted intracranially with 5×10^5 luciferase-labeled GBM cells (10 μL of PBS) using a stereotactic device. The injection site was located 2 mm lateral to the midline, 1 mm anterior to the bregma, and 2.5 mm deep. Tumor progression was assessed using an *in vivo* bioluminescence imaging platform (PerkinElmer). Euthanasia was performed by intraperitoneal injection of sodium pentobarbital (≥150 mg/kg) at humane endpoints or at study termination.

Statistical analysis

We used the R programming language to perform bioinformatics analysis. Differences in gene expression were evaluated using Student's t test. Kaplan-Meier survival curves were constructed after the optimal cutoff values were determined with the *survminer* package. Survival differences were calculated using the log-rank test. Data visualization was performed with GraphPad Prism, and statistical comparisons were performed using unpaired t tests or one-way ANOVA, as appropriate. Data are presented as the mean ± SD. Statistical significance was defined as $P < 0.05$.

Results

ECE1c is the predominant isoform in GBM and is associated with poor prognosis

Transcriptomic profiles were obtained from the CGGA database. To identify proteins involved in CD44-mediated GBM progression, differentially upregulated genes were identified based on the mesenchymal subtype and CD44 expression levels. Subsequent co-expression analyses were conducted to identify genes correlated with CD44 and genes associated with patient prognosis. Following a cross-analysis of four gene datasets, we selected six intersecting genes, among which ECE1 was the most notable candidate (**Figures 1A-D**, S1A). Consistent results from TCGA and CGGA further demonstrated that ECE1 expression positively correlated with increasing glioma grade (Figure S1B, S1C). Single-cell RNA sequencing analysis showed that ECE1 expression was significantly higher in malignant cells than in non-malignant and immune cell populations (Figure S2A). Multivariate Cox regression analysis further demonstrated that ECE1 was independently associated with poor overall survival (*HR* = 1.29, 95% *CI*: 1.15-1.45, $P < 0.001$; Figure S2B). Additionally, pan-cancer analyses revealed that ECE1 was dysregulated across multiple tumor types and was strongly overexpressed in GBM (Figure S1D). These findings were independently validated using the TCGA (**Figures 1E** and S3A, S3B) and CGGA (**Figure 1F**) cohorts.

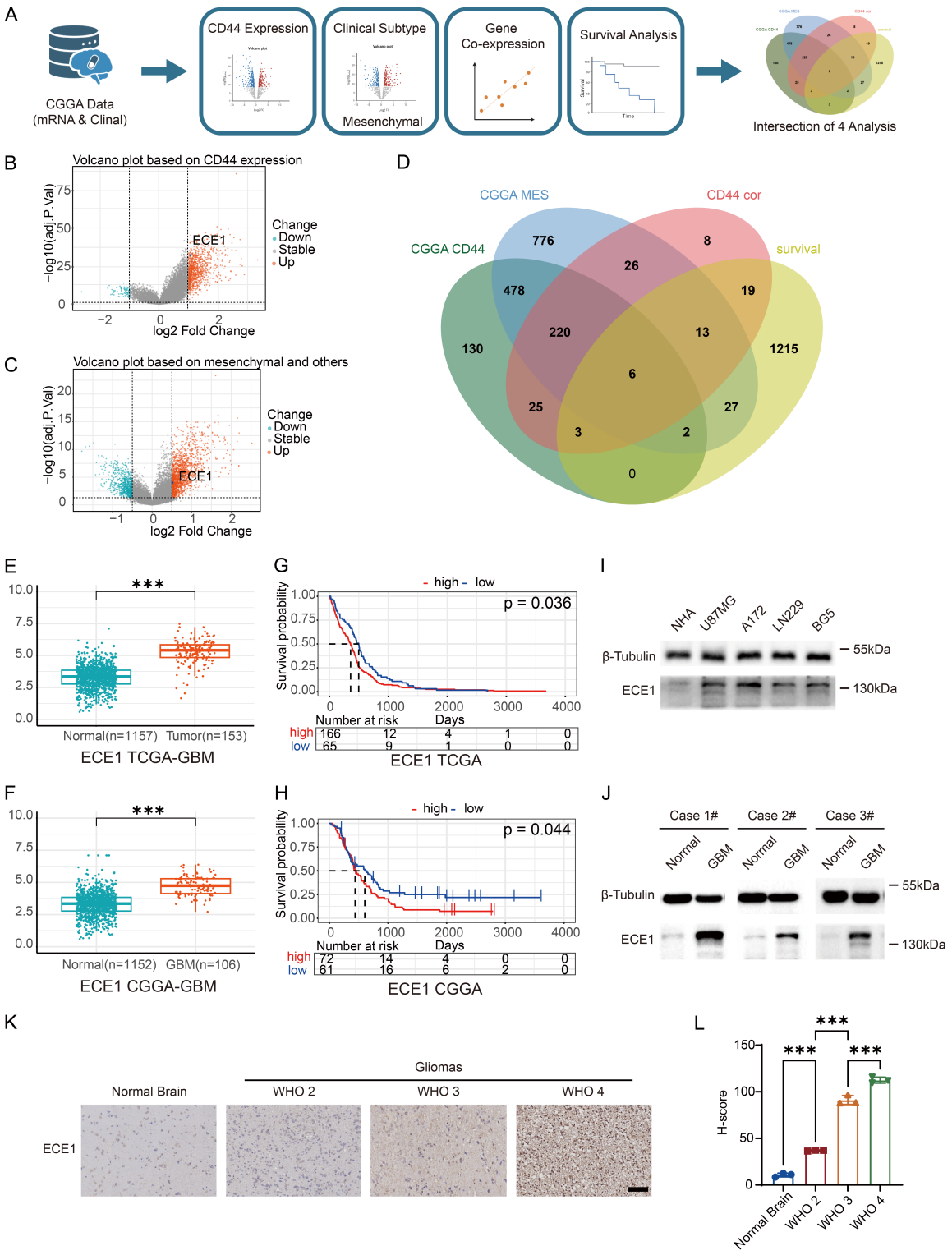

Figure 1. ECE1 expression is elevated in GBM and is correlated with malignant progression. (A) Schematic overview of the analysis: mRNA expression and clinical data from the CGGA database were analyzed using four complementary approaches: CD44 high vs. low expression, mesenchymal vs. other subtypes, CD44 coexpression analysis (Pearson's correlation test), and survival-related (Cox regression test) differentially expressed genes (DEGs). The intersection of these datasets was visualized using a Venn diagram to identify key mesenchymal- and CD44-associated genes. (B, C) Volcano plots showing DEGs between the CD44 high/low groups and the mesenchymal/other subtypes. (D) Venn diagram of the four datasets identifying six intersecting genes (GALNT2, FAM114A1, TMEM43, COLGALT1, ECE1, and SP140L). (E, F) ECE1 expression in GBM and normal tissues from the TCGA, CGGA, and GTEx

databases. (G, H) Kaplan-Meier survival curves showing that high ECE1 expression predicts poor overall survival in the TCGA and CGGA cohorts with the optimal cutoff value. (I, J) Western blot analysis of total ECE1 protein in GBM cell lines (U87MG, A172, LN229, and BG5) and patient tissues compared with normal controls (cell line: n = 3 independent experiments; patient tissues: n=3 independent experiments from 3 cases). (K, L) Representative IHC images showing elevated ECE1 expression in gliomas of different grades compared with normal brain tissues. Scale bar = 100 μm. (n = 3 biological replicates). The data are shown as the mean ± SD. ***, $P < 0.001$. Two-sample Student's *t* tests (E and F), log-rank tests (G and H) and one-way ANOVA (L) were used for data analysis.

Kaplan-Meier survival analyses based on the TCGA and CGGA datasets consistently revealed that elevated ECE1 expression was associated with significantly poorer overall survival in patients with GBM (**Figure 1G**, **1H**). This association was corroborated by GEPIA2 (Figure S3C) and GlioVis (CGGA, $P = 0.0318$) (Figure S3D). However, analyses based on the TCGA database, in which median expression was used as the cutoff, did not reach statistical significance (GlioVis, $P = 0.0691$; Xena, $P = 0.0900$) (Figure S3E, S3F). Notably, when the primary progression-free interval was used as the clinical endpoint, high ECE1 expression remained significantly associated with adverse patient outcomes (Figure S3G).

In agreement with the patient data, ECE1 expression was markedly elevated in various GBM cell lines and glioma tissues compared with normal human astrocytes and normal brain tissues (**Figure 1I-L**). The four known ECE1 isoforms (ECE1a-d) arise from alternative splicing events differing by only a few amino acids, making them difficult to distinguish using conventional antibodies. Isoform-specific qRT-PCR analysis across GBM cell lines (U87MG, A172, LN229, and GBM#BG5) demonstrated that ECE1c was the predominant transcript in GBM cells (Figure S4A). This finding is in line with those of previous reports indicating that ECE1c is the dominant isoform in other malignancies [12, 18].

Collectively, these clinical and experimental data establish ECE1c as the major functional isoform of ECE1 in GBM and suggest that it may play a critical role in glioblastoma pathogenesis and disease progression.

Knockdown of ECE1 suppresses malignant phenotypes of GBM cells in vitro

To investigate the biological role of ECE1 in GBM, its expression was inhibited in U87MG, A172, LN229, and GBM#BG5 cell lines with specific siRNAs. qRT-PCR and Western blot results (**Figure 2A** and **2B**) demonstrated that ECE1 knockdown effectively reduced ECE1 expression at both the mRNA and protein levels.

Cell viability assays revealed a significant decrease in cell proliferation following ECE1 silencing (**Figure 2C**). Consistently, EdU incorporation experiments revealed a notable reduction in the percentage of proliferating nuclei (**Figure 2D**, **2E**), confirming that ECE1 deletion hinders GBM cell growth. Additionally, neurosphere formation and extreme limiting dilution assays revealed that knocking down ECE1 greatly reduced the self-renewal capacity of GBM#BG5 cells (**Figure 2F-H**), suggesting that ECE1 plays a role in maintaining glioma stem-like characteristics.

Considering the extremely invasive characteristics of GBM, we next investigated the effect of ECE1 silencing on cellular motility. Transwell migration studies (**Figure 3A**, **3B**) and wound-healing assays (**Figure 3E**, **3F**) both revealed that, compared with control cells, ECE1 knockdown cells were significantly less migratory. In three-dimensional spheroid invasion studies, compared with control spheroids, which demonstrated significant radial infiltration into the surrounding matrix, ECE1-deficient cells generated compact spheroids with restricted invasive fronts (**Figure 3C**, **3D**).

These findings strongly suggest that ECE1 promotes the growth, self-renewal, and invasion of GBM cells *in vitro*, indicating that ECE1 is an important factor in making glioblastoma more malignant.

ECE1c facilitates GBM invasion through the ROCK2-MYH10 axis

After confirming that ECE1 controls the cancerous behavior of GBM cells *in vitro*, we proceeded to elucidate its molecular mechanism. ECE1 functions as a metalloprotease that converts big endothelin-1 (big ET-1) into the bioactive

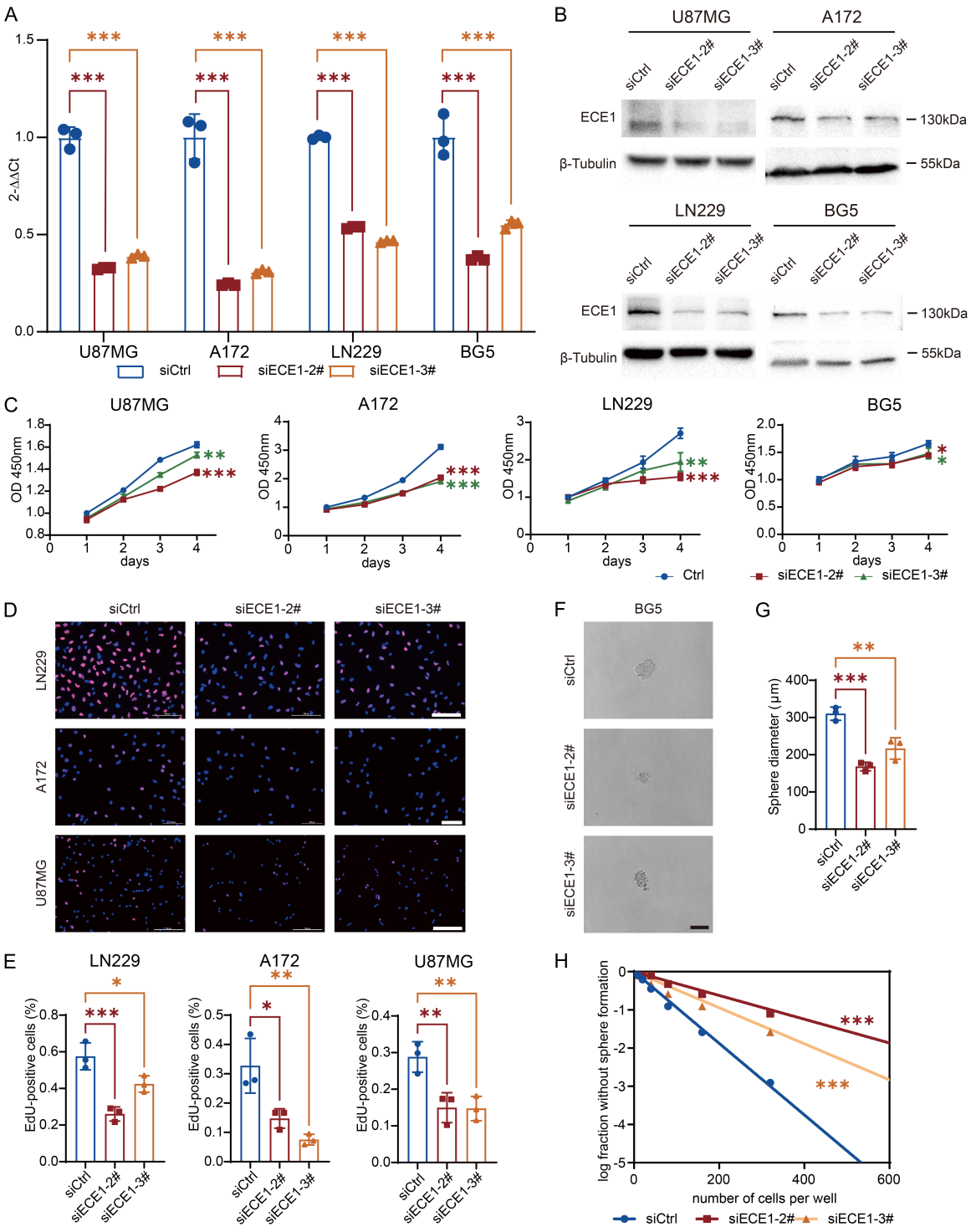

Figure 2. Knockdown of ECE1 expression suppresses GBM cell proliferation. (A, B) qRT-PCR and Western blot validation of ECE1 knockdown efficiency in U87MG, A172, LN229, and BG5 cells (qRT-PCR: n = 3 independent experiments; WB: n = 3 independent experiments). (C) CCK-8 assay showing reduced cell viability following ECE1 silencing (n = 3 independent experiments). (D, E) Representative images and quantification of EdU assays demonstrating decreased proliferative activity after ECE1 knockdown (n = 3 independent experiments). Scale bar = 100 μm. (F, G) Neurosphere formation assay showing impaired self-renewal capacity upon ECE1 depletion. Scale bar = 100 μm. (n = 3 independent experiments). (H) Limiting dilution analysis indicating a reduced sphere-forming frequency following ECE1 knockdown (n = 15 independent experiments). The data are shown as the mean ± SD. *, $P < 0.05$; **, $P < 0.01$; ***, $P < 0.001$. One-way ANOVA (A, C, E, and G) and pairwise tests (H) were used for data analysis.

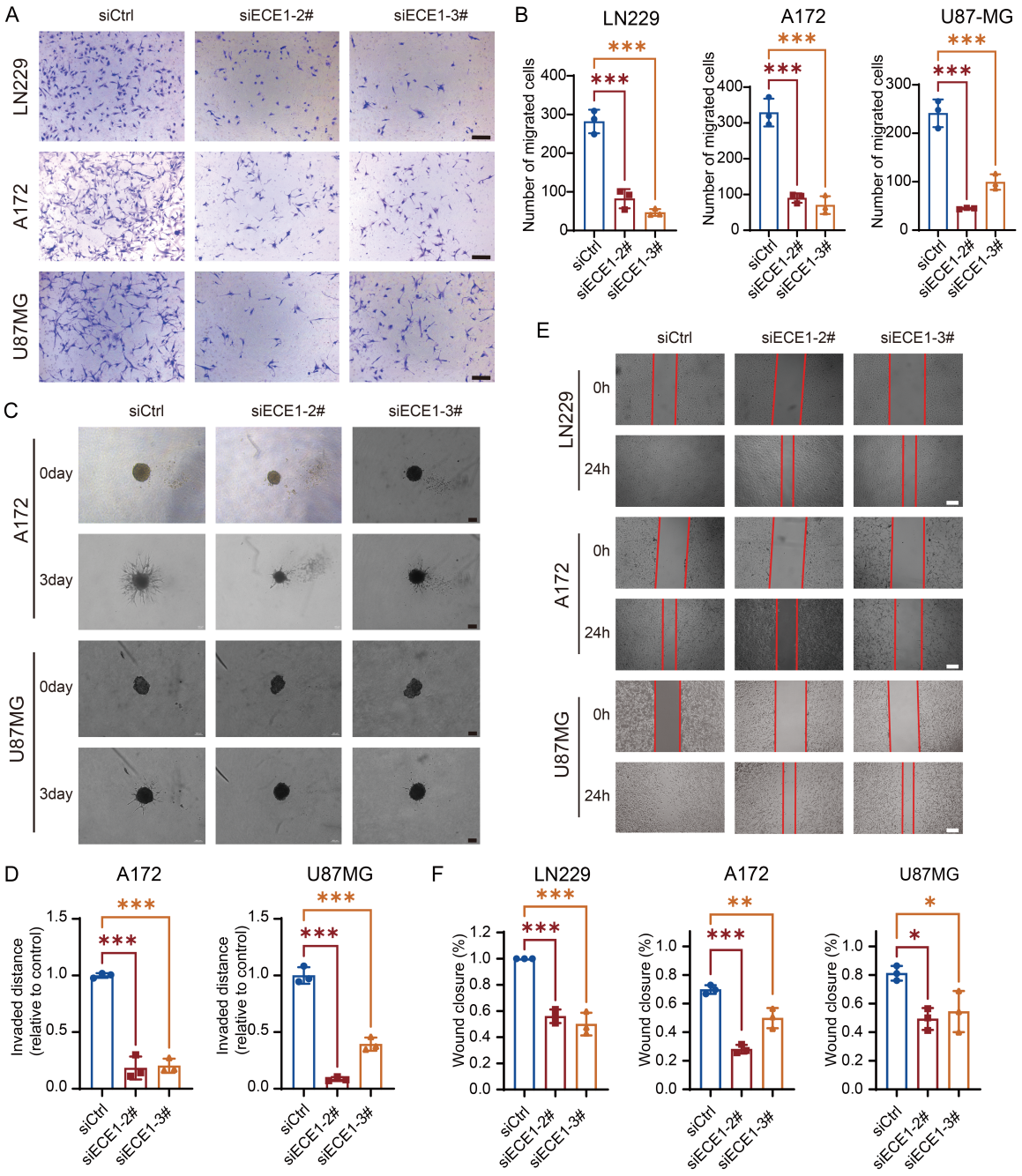

Figure 3. Knocking down of ECE1 expression suppresses GBM cell migration and invasion *in vitro*. (A, B) Transwell migration assays showing significantly reduced migratory capacity after ECE1 silencing. Scale bar = 100 μm. (n = 3 independent experiments). (C, D) Matrigel invasion assays demonstrating impaired invasive potential following ECE1 knockdown (n = 3 independent experiments). Scale bar = 100 μm. (E, F) Wound-healing assays showing decreased migration upon ECE1 depletion. Scale bar = 100 μm. (n = 3 independent experiments). The data are shown as the mean ± SD. *, $P < 0.05$; **, $P < 0.01$; ***, $P < 0.001$. One-way ANOVA (B, D and F) was used for data analysis).

peptide ET-1. However, the role of ET-1 signaling in GBM remains debated. Supplementation with exogenous ET-1 did not restore the decrease in cell viability induced by ECE1 knockdown (Figure S4B), indicating that ECE1 may have ET-1-independent effects on GBM.

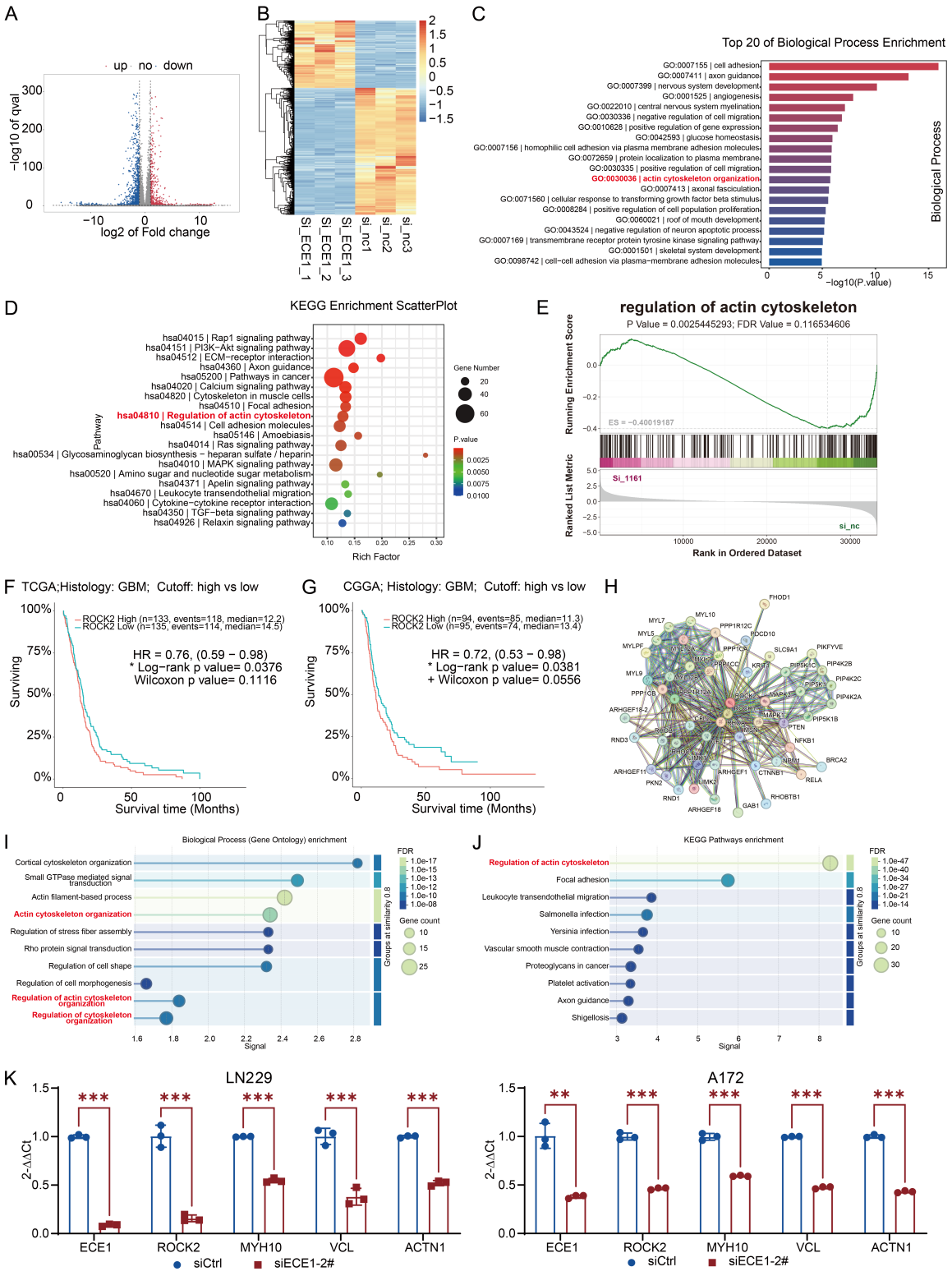

Figure 4. ECE1 regulates cytoskeletal remodeling. (A, B) Volcano plot and heatmap of differentially expressed genes in LN229 cells after ECE1 knockdown, as determined by RNA sequencing. (C) Gene Ontology (GO) analysis of the top 20 significantly enriched biological processes. (D, E) KEGG and GSEA analyses indicating significant enrichment of the "regulation of the actin cytoskeleton" pathway. (F, G) Kaplan-Meier survival analyses of the TCGA and CGGA datasets showing that high ROCK2 expression is correlated with poor overall survival in patients with GBM. (H-J) GO and KEGG analyses using STRING revealing that ROCK2 is closely associated with actin cytoskeleton regulation. (K) qRT-PCR analysis of cytoskeleton-related genes (ROCK2, MYH10, VCL, and ACTN1) in LN229 and A172 cells following ECE1 knockdown (n = 3 independent experiments). The data are shown as the mean ± SD. An unpaired *t* test (K) was used for data analysis. **, $P < 0.01$; ***, $P < 0.001$.

To clarify the pathways that facilitate ECE1-induced malignancy, we conducted transcriptome sequencing after ECE1 knockdown in LN229 cells. Differential expression analysis (**Figure 4A**, **4B**) revealed enrichment of genes associated with the "regulation of the actin cytoskeleton" pathway, corroborated by both GO (**Figure 4C**) and KEGG (**Figure 4D**) analyses. Gene set enrichment analysis (GSEA) revealed a strong association between ECE1 expression and cytoskeletal regulation (P = 0.0025; FDR = 0.1165) (**Figure 4E**).

The validation of the RNA-seq results using qRT-PCR demonstrated that the silencing of ECE1 in LN229 and A172 cells resulted in the downregulation of the expression of various actin-associated regulators, including ROCK2, MYH10 (myosin heavy chain 10), VCL, and ACTN1 (**Figure 4K**). Conversely, overexpression of ECE1c upregulated the same genes (Figure S4C, S4D). ROCK2 was identified as a critical regulator of the actin cytoskeleton (Figure S5A). Bioinformatic analyses of TCGA and CGGA data indicated that ROCK2 expression was linked to unfavorable prognosis in GBM and correlated with the modulation of the actin cytoskeleton (**Figure 4F-J**).

In line with these results, knocking down ECE1 led to lower levels of ROCK2 and proteins linked to invasion, such as MYH10, MMP2, N-cadherin, and Slug (**Figure 5A**). ROCK2 overexpression not only increased the expression of these invasion markers but also mitigated the inhibitory effects resulting from ECE1 deletion (**Figure 5A**). To further clarify the hierarchical link, we performed epistasis analysis and found that the knockdown of ROCK2 reduced the expression of its downstream targets (MYH10, MMP2, N-cadherin, and Slug) without altering ECE1 levels (**Figure 5B**). Moreover, the overexpression of ECE1c did not restore the expression of these proteins upon the silencing of ROCK2. Transwell experiments revealed that knocking down ECE1 expression significantly inhibited GBM cell invasion, whereas overexpressing ROCK2 increased invasion and partly reversed the inhibitory effect (**Figure 5C**, **5D**). Finally, consistent with the ET-1-independent mechanism, exogenous ET-1 supplementation failed to restore invasion after ECE1 knockdown (**Figure 5E**, **5F**).

Collectively, these data demonstrate that ECE1c promotes GBM invasiveness through the ROCK2-MYH10 signaling axis, independent of canonical ET-1 signaling.

ECE1c mechanistically regulates GBM invasion via interaction with ACTB

Because ECE1c promotes cell invasion by controlling the cytoskeleton, we wanted to identify its interacting molecular partners. We used LN229 cell lysates and an anti-ECE1 antibody to perform coimmunoprecipitation followed by mass spectrometry (Co-IP/MS). Pathway analysis using KEGG (**Figure 6A**) and GO (**Figure 6B**) for the interacting proteins revealed that the "regulation of actin cytoskeleton" pathway was enriched. STRING protein-protein interaction mapping revealed that ACTB was a key node in this network (Figure S5B).

Reciprocal Co-IP experiments in both LN229 and A172 cells confirmed this connection, demonstrating the mutual linkage between ECE1 and ACTB (**Figure 6C**, **6D**). Immunofluorescence labeling revealed clear colocalization of ECE1 and ACTB in the cytoplasm of GBM cells (**Figure 6E**).

Phenotypic investigations demonstrated that control GBM cells displayed pronounced lamellipodia and filopodia, indicating active actin remodeling and invasive activity (**Figure 6F**). In contrast, cells lacking ECE1 exhibited a marked decrease in membrane protrusions, whereas ECE1c overexpression strongly promoted their development (**Figure 6F**, **6G**).

These findings demonstrate that ACTB binds to ECE1c, elucidating the molecular foundation for ECE1c-mediated actin polymerization and pseudopodia extension. This association supports a model in which ECE1c promotes GBM invasion via actin cytoskeletal remodeling downstream of the ROCK2-MYH10 axis and through interaction with ACTB.

ECE1c promotes invasive malignant progression of GBM in vivo

To determine whether ECE1c enhances GBM malignancy *in vivo*, we developed orthotopic xenograft models in nude mice utilizing luciferase-labeled LN229 cells with stable ECE1 knockdown (shECE1) or ECE1c overexpression (oeECE1c) (**Figure 7A**, **7B**). Bioluminescence

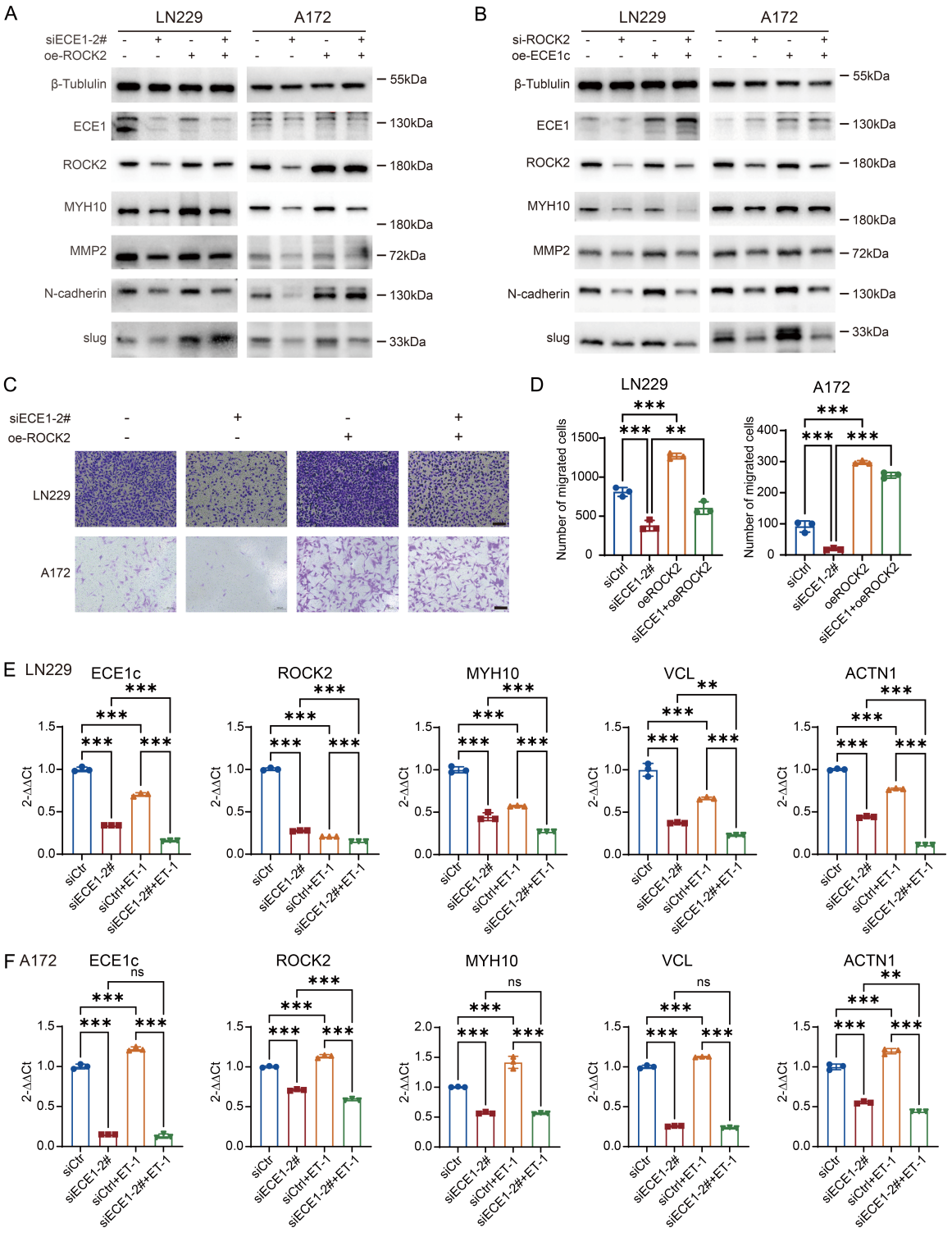

Figure 5. ECE1c modulates ROCK2 to regulate cytoskeletal remodeling. (A) Immunoblot analysis showing that ECE1 knockdown decreases the expression of ROCK2, MYH10, MMP2, N-cadherin, and Slug. Rescue experiments demonstrated that ectopic ROCK2 expression partially restores the invasive capacity of ECE1-silenced GBM cells (n = 3 independent experiments). (B) Western blot analysis showing that ROCK2 knockdown reduces MYH10, MMP2, N-cadherin, and Slug levels, while ECE1 expression remains unchanged. Overexpression of ECE1c does not reverse the effects of ROCK2 silencing (n = 3 independent experiments). (C, D) Transwell assays showing that ECE1 silencing suppresses invasion, whereas ROCK2 overexpression restores invasive ability. Scale bar = 100 μm. (n = 3 independent experiments). (E, F) qRT-PCR analysis showing that supplementation with exogenous endothelin-1 (ET-1) fails to rescue the altered expression of cytoskeleton-related genes following ECE1 knockdown (n = 3 independent experiments). The data are shown as the mean ± SD. One-way ANOVA (D-F) was used for data analysis. *ns*, not significant; **, $P < 0.01$; ***, $P < 0.001$.

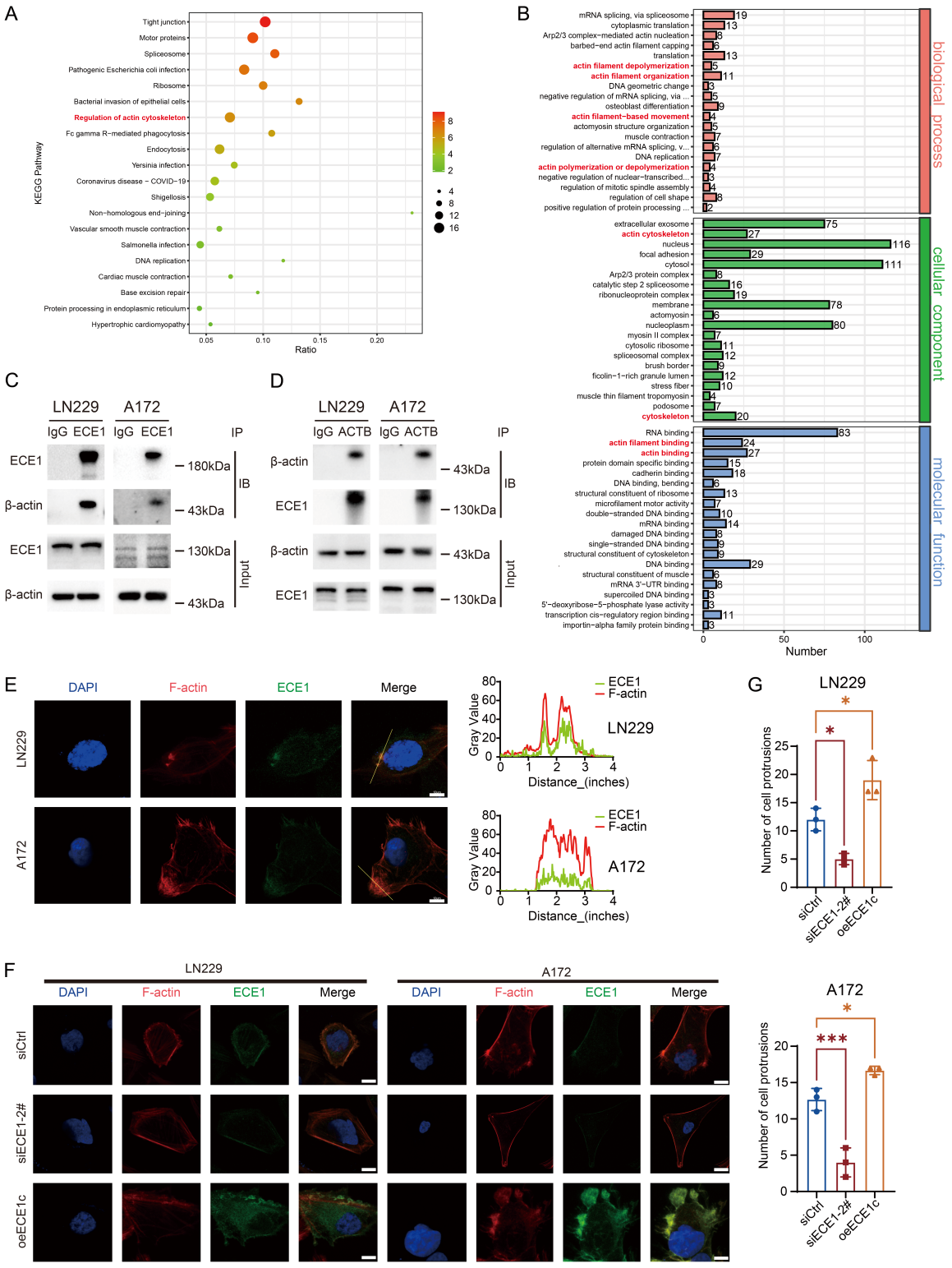

Figure 6. ECE1 interacts with ACTB to regulate cytoskeletal remodeling and promote GBM invasiveness. (A) KEGG and (B) GO analyses of ECE1-interacting proteins consistently revealed enrichment in the "regulation of the actin cytoskeleton" pathway. (C, D) Coimmunoprecipitation (Co-IP) assays demonstrating a specific interaction between ECE1 and ACTB in GBM cell lysates. ECE1 was successfully pulled down with ACTB, and reciprocal immunoprecipitation confirmed that ACTB could also precipitate ECE1 (n = 3 independent experiments). (E) Representative immunofluorescence images of GBM cells showing the colocalization of ECE1 (green) with F-actin (red). Nuclei were

counterstained with DAPI (blue). Scale bar = 10 μm. (n = 3 independent experiments). (F, G) Representative confocal images showing reduced pseudopodia formation following ECE1 knockdown and enhanced protrusive activity upon ECE1c overexpression. Quantification of the number of pseudopodia per cell is shown. Scale bar = 10 μm. (n = 3 independent experiments). The data are shown as the mean ± SD. One-way ANOVA (G) was used for data analysis. *, $P < 0.05$; ***, $P < 0.001$.

imaging was used to monitor intracranial tumor progression skull over time.

Four weeks after implantation, compared with control mice, mice with shECE1 tumors developed significantly smaller tumors, whereas mice with oeECE1c tumors developed significantly larger tumors (**Figure 7C**, **7D**). Kaplan-Meier survival analysis corroborated these data, revealing that mice in the shECE1 group exhibited considerably extended longevity, whereas those in the oeECE1c group had a reduced median survival time (**Figure 7E**).

Histopathological examination using hematoxylin and eosin (H&E) staining revealed that ECE1 depletion suppressed infiltrative tumor growth, but ECE1c overexpression enhanced the invasive phenotype (**Figure 7F**, **7G**). We assessed the effect of ECE1c on GBM invasion *in vivo* using H&E-stained sections [33]. The number of invasive finger-like protrusions at the tumor-brain interface was quantified. These results indicate that ECE1c expression is associated with enhanced intracranial invasive behavior of GBM cells (**Figure 7G**). Immunohistochemical analysis corroborated these findings, revealing a significant reduction in the proliferative marker Ki67 in shECE1 tumors and an increase in oeECE1c tumors, reflecting diminished and heightened proliferative activity, respectively. Changes in the levels of ECE1 expression were similar in tumor tissues.

These *in vivo* results provide substantial evidence that ECE1c promotes GBM tumor growth, invasion, and malignant development.

Discussion

In this investigation, we identified ECE1c as a crucial regulator of GBM malignancy. We demonstrated that ECE1c is the predominant isoform in GBM cells and that its depletion significantly impedes growth, motility, and invasion both *in vitro* and *in vivo*. Mechanistically, ECE1c initiates a novel ROCK2-MYH10 signaling pathway that reorganizes the actin cytoskeleton, promotes pseudopodia formation, and enhances invasive growth. Furthermore, ECE1c interacts with ACTB, facilitating actin filament assembly and sustaining the invasive cytoskeletal architecture of GBM cells (**Figure 8**). These results demonstrate that, in addition to its established enzymatic function in endothelin-1 (ET-1) the activation, ECE1c exerts oncogenic effects in GBM.

Additionally, four isoforms of ECE1 (ECE1a-d) are generated through alternative promoter usage and splicing [12, 15, 34, 35]. Although the N-terminal regions of these isoforms differ only slightly, such small variations strongly affect their subcellular localization and function [18, 36]. Our results indicate that ECE1c is the predominant isoform expressed in GBM cell lines, which aligns with prior observations in other malignancies, including prostate and colorectal cancers [18, 20]. Notably, CK2-mediated phosphorylation of the C-terminal serine residue of ECE1c stabilizes the protein, preventing proteasomal degradation and increasing tumor cell invasion [22]. The ECE1cK6R mutant, which is not present in GBM, has been shown to increase ECE1c stability and improve chemoresistance and invasion. However, the exact way in which ECE1c promotes glioma malignancy is still unclear [37]. The high expression of this isoform in GBM suggests that it may possess enhanced stability and contribute to intracranial tumor progression.

Historically, ECE1 has been described as a membrane metalloprotease that cleaves big ET-1 into bioactive ET-1, a potent vasoactive peptide involved in tumor angiogenesis and proliferation [11, 15, 38]. Nevertheless, accumulating evidence indicates that pharmacological inhibition of ECE1 can impede tumor growth without affecting ET-1 levels, and exogenous ET-1 supplementation fails to counteract this inhibitory effect, suggesting the involvement of ET-1-independent mechanisms [12, 37]. In line with these observations, our results demonstrate that ECE1 promotes tumorigenesis independently of ET-1 signaling, serving as a key regulator of cytoskeletal signaling. ECE1 facili-

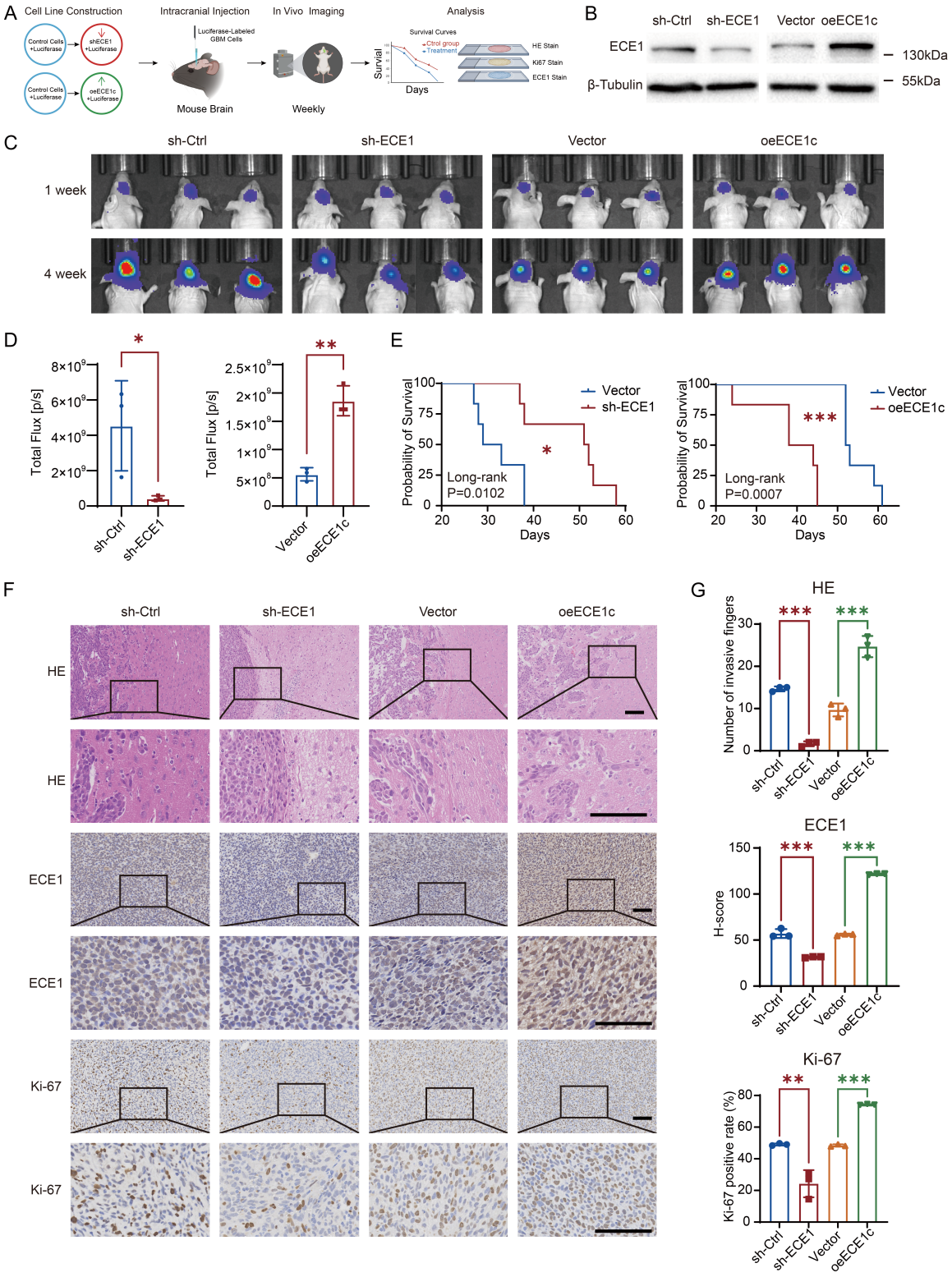

Figure 7. ECE1c promotes GBM tumor progression *in vivo*. (A) Schematic illustration of intracranial implantation of luciferase-labeled GBM cells (control, ECE1 knockdown, or ECE1c overexpression) to establish orthotopic xenograft models. (B) Immunoblot verification of the ECE1 knockdown or ECE1c overexpression efficiency in the LN229 cell line (n = 3 independent experiments). (C, D) Quantification of tumor bioluminescence intensity at 4 weeks post-implantation (n = 3 biological experiments). (E) Kaplan-Meier survival analysis of nude mice bearing tumors (n = 6 mice per group). (F) Representative H&E, Ki-67, and ECE1 immunohistochemical staining of brain sections showing

tumor boundaries, proliferative activity, and ECE1 expression levels. Scale bar = 100 μm. (n = 3 biological experiments). (G) Invasive finger-like protrusions at the tumor-brain interface were quantified in H&E-stained sections. ECE1 expression was semi-quantitatively assessed using the H-score method, and the Ki-67 labeling index was calculated as the percentage of Ki-67 positive tumor cells. The data are shown as the mean ± SD. Unpaired *t* tests (D, G) and the log-rank test (E) were used for data analysis. *, $P < 0.05$; **, $P < 0.01$; ***, $P < 0.001$.

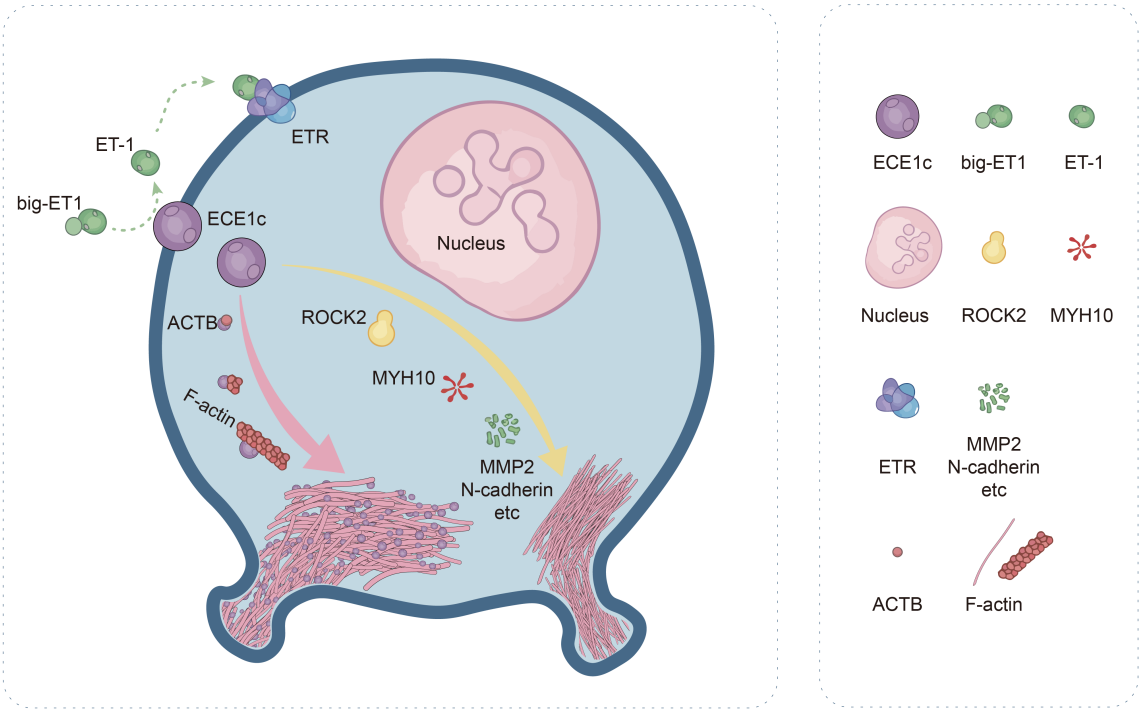

Figure 8. Proposed model illustrating how ECE1c promotes glioblastoma (GBM) progression. ECE1c, the predominant isoform of ECE1 in GBM, interacts with ACTB and modulates ROCK2 to activate cytoskeletal remodeling pathways independent of endothelin-1 (ET-1) signaling. Through these axes, ECE1c enhances pseudopodia formation, thereby facilitating tumor cell migration and invasion. In both in vitro and in vivo studies, knockdown of ECE1 disrupts cytoskeletal organization, reduces invasive potential, and inhibits tumors from growing. This model highlights that targeting ECE1c could represent a potential strategy to limit the aggressive behavior of GBM.

tates the assembly of actomyosin networks that drive cell contraction, migration, and invasion by modulating ROCK2 expression and interacting with ACTB. This cytoskeleton-related function highlights the multifaceted role of ECE1 in promoting tumor aggressiveness.

ROCK2 is a well-known regulator of actin cytoskeletal remodeling, stress fibers formation, and cell motility [23]. Its activation increases myosin heavy chain expression and actomyosin contractility, both of which are critical for tumor invasion [39-42]. Nonmuscle myosin heavy chain IIB (NMHC IIB), encoded by the MYH10 gene and constituting the component of nonmuscle myosin IIB (NM IIB), is essential for tumor invasion because it regulates cytoskeletal dynamics, enhances migratory and invasive capabilities, facilitates cellular mechanotransduction, and mediates drug resistance. Dysregulated MYH10 expression has consequently been linked to malignant progression in many cancers, including ovarian and lung carcinomas [43]. Furthermore, the ROCK-MYH10 axis promotes an amoeboid invasion pattern associated with poor patient prognosis [42], and suppression of MYH10 expression reduces the invasive potential of GBM [44]. ROCK2 overexpression partially rescued the phenotypic effects induced by ECE1 depletion, suggesting that ECE1c regulates GBM invasion through multiple downstream pathways. The ROCK2-MYH10 axis appears to be an important, though not exclusive, effector. Consistently, our

data show that ECE1c affects both ROCK2 and MYH10 and also interacts with ACTB and colocalizes with F-actin. The coordinated regulation of both the upstream kinase (ROCK2) and the structural polymer (ACTB) highlights an important signaling pathway through which ECE1c influences cytoskeletal remodeling and promotes GBM invasiveness.

The extremely infiltrative nature of GBM remains the fundamental hurdle to curative therapy, as diffuse invasion into neighboring brain parenchyma limits complete surgical resection [45, 46]. Increasing evidence suggests that regulation of actin cytoskeletal dynamics is a key component of this process, as it controls cell shape, polarity, and motility [47]. Consistent with this model, loss of ECE1 disrupts F-actin organization, reduces pseudopodia formation, and inhibits cell motility, demonstrating its critical role in cytoskeletal regulation. Because highly motile GBM cells frequently exhibit increased resistance to radiation and chemotherapy [48], inhibiting ECE1 may represent a viable strategy to suppress tumor progression.

The identification of ECE1c as a cytoskeletal regulator presents novel therapeutic opportunities. Small-molecule inhibitors of ECE1 have been developed for cardiovascular diseases [49, 50], but their potential anticancer effects remain insufficiently explored. Our results suggest that ECE1 inhibition may suppress GBM invasion independently of ET-1 inhibition, providing a safer and more targeted therapeutic strategy. Moreover, disrupting the interaction between ECE1 and ACTB may selectively impair tumor cell motility while preserving physiological ET-1 processing in normal tissues. The development of peptide mimetics or small molecules that block this interaction may therefore represent a promising therapeutic strategy for GBM and potentially other highly aggressive malignancies.

This study has several limitations. The interaction between ECE1 and ACTB was validated based on biochemical association rather than direct structural evidence; and the precise binding domains and structural interface remain to be elucidated. Advanced techniques such as cryo-electron microscopy or domain-mapping mutagenesis will be required to characterize these molecular interactions. Additionally, although our *in vivo* model demonstrated reduced tumor progression following ECE1 knockdown, orthotopic models incorporating invasive tracking may more accurately represent the dynamics of tumor infiltration within the brain environment. Future studies should also evaluate the relationship between ECE1 expression and treatment resistance in clinical cohorts.

Conclusions

In conclusion, our findings demonstrate that ECE1c is a key regulator of GBM invasion and progression. By activating the ROCK2-MYH10 signaling axis and interacting with ACTB, ECE1c strongly regulates cytoskeletal remodeling and pseudopodia formation, thereby promoting GBM cell invasion. Targeting this pathway, particularly by disrupting ECE1-cytoskeleton interactions, may represent a novel and effective therapeutic strategy for glioblastoma.

Availability of data and materials

The data generated in this study are available from the corresponding author upon reasonable request. Proteomics data generated by mass spectrometry have been submitted to the ProteomeXchange Consortium via the PRIDE [51] partner repository. The dataset identifier is PXD071913. RNA sequencing data have been deposited in the NCBI Sequence Read Archive (SRA) under the BioProject accession PRJNA1377472.

Acknowledgements

We are grateful to LC Bio Technology Co., Ltd. for assisting in sequencing and bioinformatics analysis. This work was supported by Key R&D Program of Shandong Province [2025CXPT177], Shandong Provincial Laboratory Project [SYS202202], Special Foundation for Taishan Scholars [tshw201502056], and the Incubating Foundation of the Second Qilu Hospital of Shandong University [2023YP04].

Disclosure of conflict of interest

None.

Abbreviations

GBM, Glioblastoma multiforme; IHC, Immunohistochemistry; MES, mesenchymal; MMP, matrix metalloproteinase; ECE, endothelin-con-

verting enzyme; GSEA, Gene set enrichment analysis; NHA, normal human astrocytes; ET, endothelin; CK2, casein kinase 2; KEGG, Kyoto Encyclopedia of Genes and Genomes; EMT, epithelial-mesenchymal transition; Co-IP, Co-immunoprecipitation; ROCK2, Rho-associated coiled-coil containing protein kinase 2; EGF, epidermal growth factor; siRNA, small interfering RNA; IF, Immunofluorescence; qRT-PCR, quantitative real-time PCR; NM IIB, nonmuscle myosin IIB; GO, Gene Ontology; bFGF, basic fibroblast growth factor; MYH10, myosin heavy chain 10.

Ethics statement

Animal experiments were conducted in accordance with applicable laws, regulations, and institutional guidelines, approved by the Ethics Committee of Qilu Hospital of Shandong University (DWLL-2021-115). Human glioma samples were collected from surgical patients at the second Qilu Hospital, approved by the Ethics Committee of the second Qilu Hospital of Shandong University (KYLL2024230). Non-tumor brain tissues were collected from patients undergoing internal decompression surgery due to severe craniocerebral trauma. Written informed consent was obtained from all participants prior to sample collection.

Address correspondence to: Bin Huang and Xingang Li, Department of Neurosurgery, Qilu Hospital of Shandong University, #107 Wenhua Xi Road, Jinan 250012, Shandong, China. Tel: +86-18560085770; E-mail: hb@sdu.edu.cn (BH); Tel: +86-18560086999; E-mail: lixg@sdu.edu.cn (XGL)

References

[1] Read RD, Tapp ZM, Rajappa P and Hambardzumyan D. Glioblastoma microenvironment-from biology to therapy. Genes Dev 2024; 38: 360-379.

[2] Omuro A and DeAngelis LM. Glioblastoma and other malignant gliomas: a clinical review. JAMA 2013; 310: 1842-1850.

[3] Stupp R, Taillibert S, Kanner A, Read W, Steinberg D, Lhermitte B, Toms S, Idbaih A, Ahluwalia MS, Fink K, Di Meco F, Lieberman F, Zhu JJ, Stragliotto G, Tran D, Brem S, Hottinger A, Kirson ED, Lavy-Shahaf G, Weinberg U, Kim CY, Paek SH, Nicholas G, Bruna J, Hirte H, Weller M, Palti Y, Hegi ME and Ram Z. Effect of tumor-treating fields plus maintenance temozolomide vs maintenance temozolomide alone on survival in patients with glioblastoma: a randomized clinical trial. JAMA 2017; 318: 2306-2316.

[4] Ratliff M, Karimian-Jazi K, Hoffmann DC, Rauschenbach L, Simon M, Hai L, Mandelbaum H, Schubert MC, Kessler T, Uhlig S, Dominguez Azorin D, Jung E, Osswald M, Solecki G, Maros ME, Venkataramani V, Glas M, Etminan N, Scheffler B, Wick W and Winkler F. Individual glioblastoma cells harbor both proliferative and invasive capabilities during tumor progression. Neuro Oncol 2023; 25: 2150-2162.

[5] White J, White MPJ, Wickremesekera A, Peng L and Gray C. The tumour microenvironment, treatment resistance and recurrence in glioblastoma. J Transl Med 2024; 22: 540.

[6] Eisenbarth D and Wang YA. Glioblastoma heterogeneity at single cell resolution. Oncogene 2023; 42: 2155-2165.

[7] Minata M, Audia A, Shi J, Lu S, Bernstock J, Pavlyukov MS, Das A, Kim SH, Shin YJ, Lee Y, Koo H, Snigdha K, Waghmare I, Guo X, Mohyeldin A, Gallego-Perez D, Wang J, Chen D, Cheng P, Mukheef F, Contreras M, Reyes JF, Vaillant B, Sulman EP, Cheng SY, Markert JM, Tannous BA, Lu X, Kango-Singh M, Lee LJ, Nam DH, Nakano I and Bhat KP. Phenotypic plasticity of invasive edge glioma stem-like cells in response to ionizing radiation. Cell Rep 2019; 26: 1893-1905, e7.

[8] Bhat KPL, Balasubramaniyan V, Vaillant B, Ezhilarasan R, Hummelink K, Hollingsworth F, Wani K, Heathcock L, James JD, Goodman LD, Conroy S, Long L, Lelic N, Wang S, Gumin J, Raj D, Kodama Y, Raghunathan A, Olar A, Joshi K, Pelloski CE, Heimberger A, Kim SH, Cahill DP, Rao G, Den Dunnen WFA, Boddeke HWGM, Phillips HS, Nakano I, Lang FF, Colman H, Sulman EP and Aldape K. Mesenchymal differentiation mediated by NF-κB promotes radiation resistance in glioblastoma. Cancer Cell 2013; 24: 331-346.

[9] Behnan J, Finocchiaro G and Hanna G. The landscape of the mesenchymal signature in brain tumours. Brain 2019; 142: 847-866.

[10] Oraiopoulou ME, Tzamali E, Papamatheakis J and Sakkalis V. Phenocopying glioblastoma: a review. IEEE Rev Biomed Eng 2023; 16: 456-471.

[11] Barton M and Yanagisawa M. Endothelin: 30 years from discovery to therapy. Hypertension 2019; 74: 1232-1265.

[12] Tapia JC and Niechi I. Endothelin-converting enzyme-1 in cancer aggressiveness. Cancer Lett 2019; 452: 152-157.

[13] Whyteside AR, Hinsley EE, Lambert LA, McDermott PJ and Turner AJ. ECE-1 influences prostate cancer cell invasion via ET-1-mediated

FAK phosphorylation and ET-1-independent mechanisms. Can J Physiol Pharmacol 2010; 88: 850-854.
[14] Berger Y, Dehmlow H, Blum-Kaelin D, Kitas EA, Löffler BM, Aebi JD and Juillerat-Jeanneret L. Endothelin-converting enzyme-1 inhibition and growth of human glioblastoma cells. J Med Chem 2005; 48: 483-498.
[15] Xu D, Emoto N, Giaid A, Slaughter C, Kaw S, deWit D and Yanagisawa M. ECE-1: a membrane-bound metalloprotease that catalyzes the proteolytic activation of big endothelin-1. Cell 1994; 78: 473-485.
[16] Kedzierski RM and Yanagisawa M. Endothelin system: the double-edged sword in health and disease. Annu Rev Pharmacol Toxicol 2001; 41: 851-876.
[17] Chen L, Lu Y, Zhao M, Xu J, Wang Y, Xu Q, Cao Y and Liu H. A non-canonical role of endothelin converting enzyme 1 (ECE1) in promoting lung cancer development via directly targeting protein kinase B (AKT). J Gene Med 2024; 26: e3612.
[18] Lambert LA, Whyteside AR, Turner AJ and Usmani BA. Isoforms of endothelin-converting enzyme-1 (ECE-1) have opposing effects on prostate cancer cell invasion. Br J Cancer 2008; 99: 1114-1120.
[19] Pérez-Moreno P, Quezada-Meza C, Chavez-Almarza C, Niechi I, Silva-Pavez E, Trigo-Hidalgo C, Aguayo F, Jara L, Cáceres-Verschae A, Varas-Godoy M, Díaz VM, García De Herreros A, Burzio VA and Tapia JC. Phosphorylation of endothelin-converting enzyme-1c at serines 18 and 20 by CK2 promotes aggressiveness traits in colorectal cancer cells. Front Oncol 2020; 10: 1004.
[20] Pérez-Moreno P, Indo S, Niechi I, Huerta H, Cabello P, Jara L, Aguayo F, Varas-Godoy M, Burzio VA and Tapia JC. Endothelin-converting enzyme-1c promotes stem cell traits and aggressiveness in colorectal cancer cells. Mol Oncol 2020; 14: 347-362.
[21] Almarza C, Villalobos-Nova K, Toro MA, González M, Niechi I, Brown-Brown DA, López-Muñoz RA, Silva-Pavez E, Gaete-Ramírez B, Varas-Godoy M, Burzio VA, Jara L, Aguayo F and Tapia JC. Cisplatin-resistance and aggressiveness are enhanced by a highly stable endothelin-converting enzyme-1c in lung cancer cells. Biol Res 2024; 57: 74.
[22] Niechi I, Silva E, Cabello P, Huerta H, Carrasco V, Villar P, Cataldo LR, Marcelain K, Armisen R, Varas-Godoy M, Fernandez C and Tapia JC. Colon cancer cell invasion is promoted by protein kinase CK2 through increase of endothelin-converting enzyme-1c protein stability. Oncotarget 2015; 6: 42749-42760.
[23] Barcelo J, Samain R and Sanz-Moreno V. Preclinical to clinical utility of ROCK inhibitors in cancer. Trends Cancer 2023; 9: 250-263.
[24] Mondal C, Di Martino JS and Bravo-Cordero JJ. Actin dynamics during tumor cell dissemination. Int Rev Cell Mol Biol 2021; 360: 65-98.
[25] Tang Y, He Y, Zhang P, Wang J, Fan C, Yang L, Xiong F, Zhang S, Gong Z, Nie S, Liao Q, Li X, Li X, Li Y, Li G, Zeng Z, Xiong W and Guo C. LncRNAs regulate the cytoskeleton and related Rho/ROCK signaling in cancer metastasis. Mol Cancer 2018; 17: 77.
[26] Lei MML, Leung CON, Lau EYT, Leung RWH, Ma VWS, Tong M, Lu YY, Huang CY, Zhu QH, Ng IOL, Ma S and Lee TKW. SCYL3, as a novel binding partner and regulator of ROCK2, promotes hepatocellular carcinoma progression. JHEP Rep 2023; 5: 100604.
[27] Tanaka HY, Nakazawa T, Miyazaki T, Cabral H, Masamune A and Kano MR. Targeting ROCK2 improves macromolecular permeability in a 3D fibrotic pancreatic cancer microenvironment model. J Control Release 2024; 369: 283-295.
[28] Demirdizen E, Al-Ali R, Narayanan A, Sun X, Varga JP, Steffl B, Brom M, Krunic D, Schmidt C, Schmidt G, Bestvater F, Taranda J and Turcan Ş. TRIM67 drives tumorigenesis in oligodendrogliomas through rho GTPase-dependent membrane blebbing. Neuro Oncol 2023; 25: 1031-1043.
[29] Junqueira Alves C, Hannah T, Sadia S, Kolsteeg C, Dixon A, Wiener RJ, Nguyen H, Tipping MJ, Silva Ladeira J, Fernandes da Costa Franklin P, de Paula Dutra de Nigro N, Alves Dias R, Zabala Capriles PV, Rodrigues Furtado de Mendonça JP, Slesinger PA, Costa KD, Zou H and Friedel RH. Invasion of glioma cells through confined space requires membrane tension regulation and mechano-electrical coupling via plexin-B2. Nat Commun 2025; 16: 272.
[30] Becker KN, Pettee KM, Sugrue A, Reinard KA, Schroeder JL and Eisenmann KM. The cytoskeleton effectors rho-kinase (ROCK) and mammalian diaphanous-related (mDia) formin have dynamic roles in tumor microtube formation in invasive glioblastoma cells. Cells 2022; 11: 1559.
[31] Zhao Z, Zhang KN, Wang Q, Li G, Zeng F, Zhang Y, Wu F, Chai R, Wang Z, Zhang C, Zhang W, Bao Z and Jiang T. Chinese glioma genome atlas (CGGA): a comprehensive resource with functional genomic data from chinese glioma patients. Genomics Proteomics Bioinformatics 2021; 19: 1-12.
[32] Szklarczyk D, Kirsch R, Koutrouli M, Nastou K, Mehryary F, Hachilif R, Gable AL, Fang T, Doncheva NT, Pyysalo S, Bork P, Jensen LJ and von Mering C. The STRING database in 2023: protein-protein association networks and func-

tional enrichment analyses for any sequenced genome of interest. Nucleic Acids Res 2023; 51: D638-D646.
[33] Fang R, Chen X, Zhang S, Shi H, Ye Y, Shi H, Zou Z, Li P, Guo Q, Ma L, He C and Huang S. EGFR/SRC/ERK-stabilized YTHDF2 promotes cholesterol dysregulation and invasive growth of glioblastoma. Nat Commun 2021; 12: 177.
[34] Jafri F and Ergul A. Nuclear localization of endothelin-converting enzyme-1: subisoform specificity. Arterioscler Thromb Vasc Biol 2003; 23: 2192-2196.
[35] Valdenaire O, Lepailleur-Enouf D, Egidy G, Thouard A, Barret A, Vranckx R, Tougard C and Michel JB. A fourth isoform of endothelin-converting enzyme (ECE-1) is generated from an additional promoter molecular cloning and characterization. Eur J Biochem 1999; 264: 341-349.
[36] Schweizer A, Valdenaire O, Nelböck P, Deuschle U, Dumas Milne Edwards JB, Stumpf JG and Löffler BM. Human endothelin-converting enzyme (ECE-1): three isoforms with distinct subcellular localizations. Biochem J 1997; 328: 871-877.
[37] Niechi I, Erices JI, Carrillo-Beltrán D, Uribe-Ojeda A, Torres Á, Rocha JD, Uribe D, Toro MA, Villalobos-Nova K, Gaete-Ramírez B, Mingo G, Owen GI, Varas-Godoy M, Jara L, Aguayo F, Burzio VA, Quezada-Monrás C and Tapia JC. Cancer stem cell and aggressiveness traits are promoted by stable endothelin-converting enzyme-1c in glioblastoma cells. Cells 2023; 12: 506.
[38] Kawanabe Y and Nauli SM. Endothelin. Cell Mol Life Sci 2011; 68: 195-203.
[39] Newell-Litwa KA, Badoual M, Asmussen H, Patel H, Whitmore L and Horwitz AR. ROCK1 and 2 differentially regulate actomyosin organization to drive cell and synaptic polarity. J Cell Biol 2015; 210: 225-242.
[40] Wang Y, Yang Q, Cheng Y, Gao M, Kuang L and Wang C. Myosin heavy chain 10 (MYH10) gene silencing reduces cell migration and invasion in the glioma cell lines U251, T98G, and SHG44 by inhibiting the wnt/β-catenin pathway. Med Sci Monit 2018; 24: 9110-9119.
[41] Ning Y, Zheng M, Zhang Y, Jiao Y, Wang J and Zhang S. RhoA-ROCK2 signaling possesses complex pathophysiological functions in cancer progression and shows promising therapeutic potential. Cancer Cell Int 2024; 24: 339.
[42] Samain R, Maiques O, Monger J, Lam H, Candido J, George S, Ferrari N, Kohlhammer L, Lunetto S, Varela A, Orgaz JL, Vilardell F, Olsina JJ, Matias-Guiu X, Sarker D, Biddle A, Balkwill FR, Eyles J, Wilkinson RW, Kocher HM, Calvo F, Wells CM and Sanz-Moreno V. CD73 controls myosin II-driven invasion, metastasis, and immunosuppression in amoeboid pancreatic cancer cells. Sci Adv 2023; 9: eadi0244.
[43] Newell-Litwa KA, Horwitz R and Lamers ML. Non-muscle myosin II in disease: mechanisms and therapeutic opportunities. Dis Model Mech 2015; 8: 1495-1515.
[44] Kenchappa RS, Radnai L, Young EJ, Zarco N, Lin L, Dovas A, Meyer CT, Haddock A, Hall A, Toth K, Canoll P, Nagaiah NKH, Rumbaugh G, Cameron MD, Kamenecka TM, Griffin PR, Miller CA and Rosenfeld SS. MT-125 inhibits non-muscle myosin IIA and IIB and prolongs survival in glioblastoma. Cell 2025; 188: 4622-4639, e19.
[45] Autier L, Clavreul A, Cacicedo ML, Franconi F, Sindji L, Rousseau A, Perrot R, Montero-Menei CN, Castro GR and Menei P. A new glioblastoma cell trap for implantation after surgical resection. Acta Biomater 2019; 84: 268-279.
[46] Stupp R, Hegi ME, Mason WP, van den Bent MJ, Taphoorn MJ, Janzer RC, Ludwin SK, Allgeier A, Fisher B, Belanger K, Hau P, Brandes AA, Gijtenbeek J, Marosi C, Vecht CJ, Mokhtari K, Wesseling P, Villa S, Eisenhauer E, Gorlia T, Weller M, Lacombe D, Cairncross JG and Mirimanoff RO; European Organisation for Research and Treatment of Cancer Brain Tumour and Radiation Oncology Groups; National Cancer Institute of Canada Clinical Trials Group. Effects of radiotherapy with concomitant and adjuvant temozolomide versus radiotherapy alone on survival in glioblastoma in a randomised phase III study: 5-year analysis of the EORTC-NCIC trial. Lancet Oncol 2009; 10: 459-466.
[47] Fabian C, Han M, Bjerkvig R and Niclou SP. Novel facets of glioma invasion. Int Rev Cell Mol Biol 2021; 360: 33-64.
[48] Lefranc F, Le Rhun E, Kiss R and Weller M. Glioblastoma quo vadis: will migration and invasiveness reemerge as therapeutic targets? Cancer Treat Rev 2018; 68: 145-154.
[49] Emoto N, Raharjo SB, Isaka D, Masuda S, Adiarto S, Jeng AY and Yokoyama M. Dual ECE/NEP inhibition on cardiac and neurohumoral function during the transition from hypertrophy to heart failure in rats. Hypertension 2005; 45: 1145-1152.
[50] Fu S, Ping P, Wang F and Luo L. Synthesis, secretion, function, metabolism and application of natriuretic peptides in heart failure. J Biol Eng 2018; 12: 2.
[51] Perez-Riverol Y, Bandla C, Kundu DJ, Kamatchinathan S, Bai J, Hewapathirana S, John NS, Prakash A, Walzer M, Wang S and Vizcaíno JA. The PRIDE database at 20 years: 2025 update. Nucleic Acids Res 2025; 53: D543-D553.

Table S1. Primer sequences

Human gene	Primers (5'-3')
β Tubulin	Forward: CATGGACTCTGTTCGCTCAGG
	Reverse: CCTTTGGCCCAGTTGTTACCT
ECE1a	Forward: GGCTGAATCTGTGGGAACCA
	Reverse: GGGCTGTGGAAGTTCACCTG
ECE1b	Forward: GTGTCCGCCCTGCTGTC
	Reverse: AGTACCACCAACACCACCAG
ECE1c	Forward: GGAACCCGGAGCTGGGAAT
	Reverse: GAGTCCACCAGGTCCTCCTC
ECE1d	Forward: GGAACCCCTTCCTCCAAGG
	Reverse: AGAAGTACCACCAACACCACC
ROCK2	Forward: AGCAGTTGGAACACCGGATT
	Reverse: ACCAATCACATTCTCGCCCA
MYH10	Forward: AGGGCATGTTTCGTACCGTT
	Reverse: AGGACACCGTTACAGCGAAG
ACTN1	Forward: GCATGGTGTAACTCCCACCT
	Reverse: CATCCCGGAAGTCCTCTTCG
VCL	Forward: TTGATGGGTCAAGGGGCATC
	Reverse: CACCACCTCTGCCACTGTAA

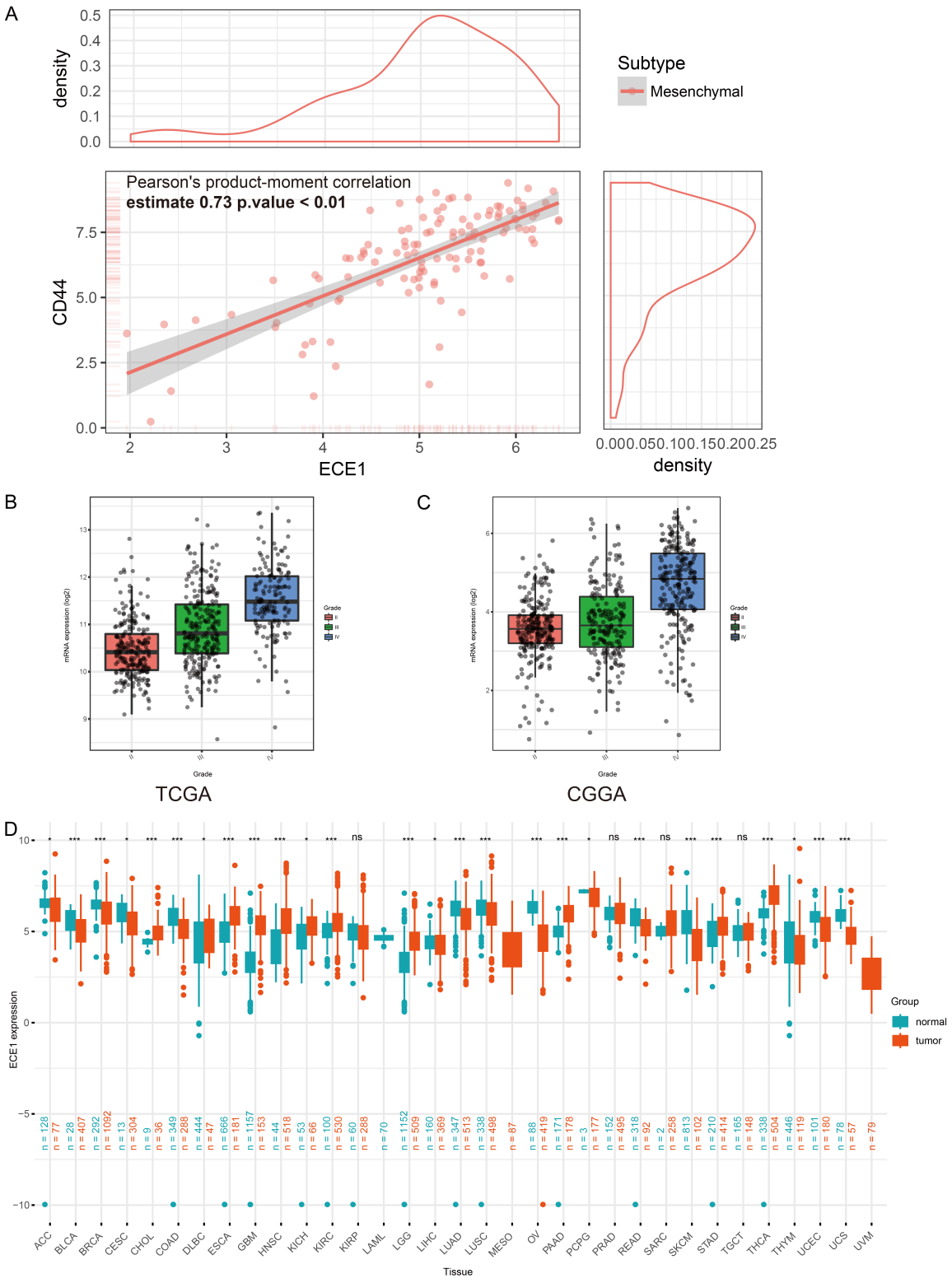

Figure S1. Correlation and expression pattern of ECE1 in GBM and pan-cancer datasets. A. Linear correlation analysis showing a positive association between CD44 and ECE1 expression in GBM. B, C. ECE1 expression across different glioma grades in TCGA and CGGA datasets was analyzed via the GlioVis platform, showing a progressive increase with tumor grade. D. Pan-cancer analysis of ECE1 expression across TCGA datasets. *ns* not significant, **P* < 0.05, ***P* < 0.01, ****P* < 0.001; two-sample Student's *t*-test D was used for data analysis.

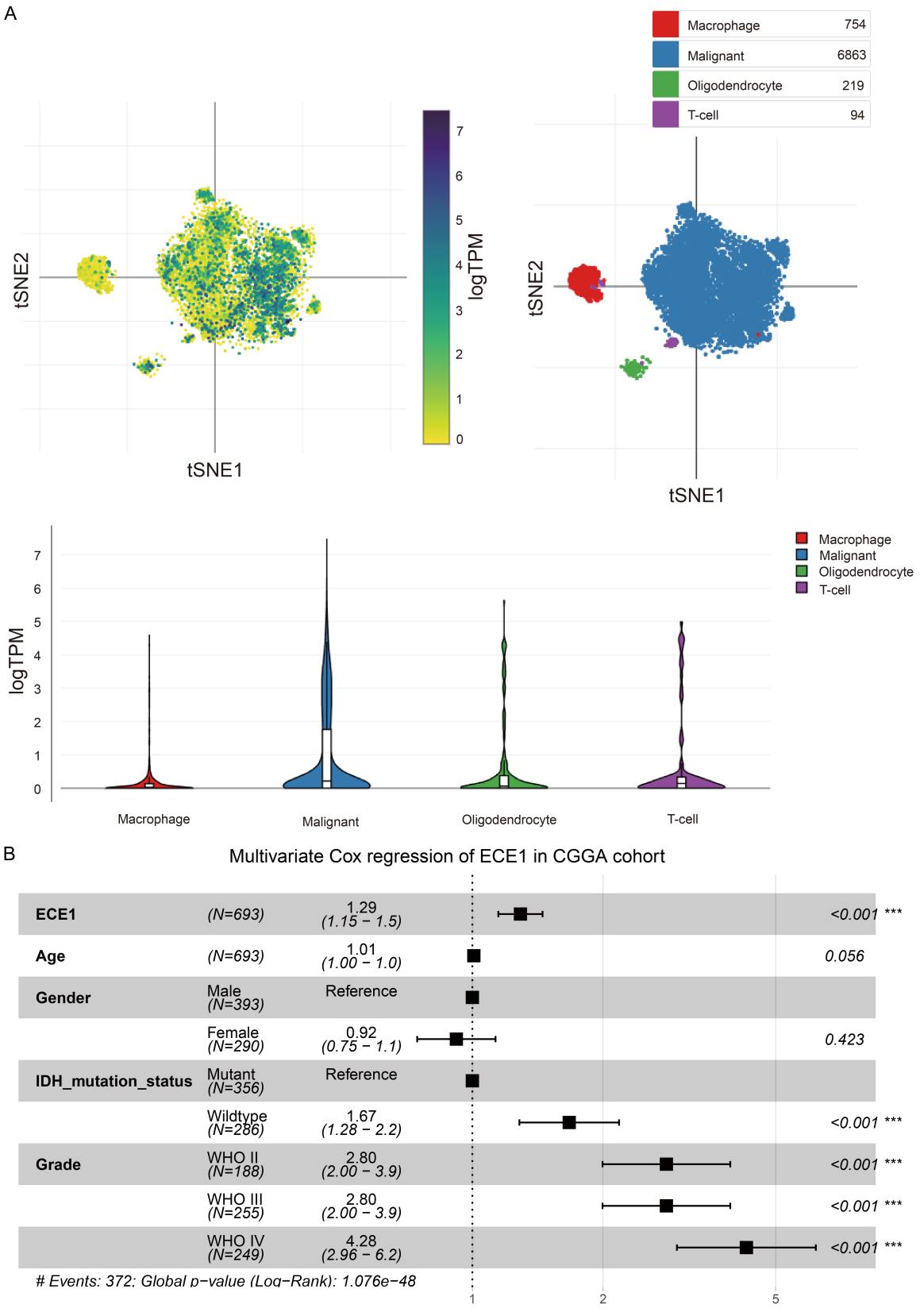

Figure S2. Distribution of ECE1 expression in single-cell sequencing and multivariate Cox regression analysis. A. Single-cell RNA-sequencing analysis of the public GSE131928 dataset demonstrated that the expression of ECE1

was significantly higher in malignant tumor cells compared with macrophages, T cells, and oligodendrocytes, as visualized by t-SNE plots and violin plots. B. Prognostic significance of ECE1 expression was evaluated using the CGGA mRNA-seq_693 cohort. Multivariate Cox regression analysis adjusted for age, sex, isocitrate dehydrogenase (IDH) mutation status, and WHO grade showed that high ECE1 expression remained independently associated with poor overall survival (*HR* = 1.29, 95% *CI:* 1.15-1.45, *P* < 0.001). ***P* < 0.001.

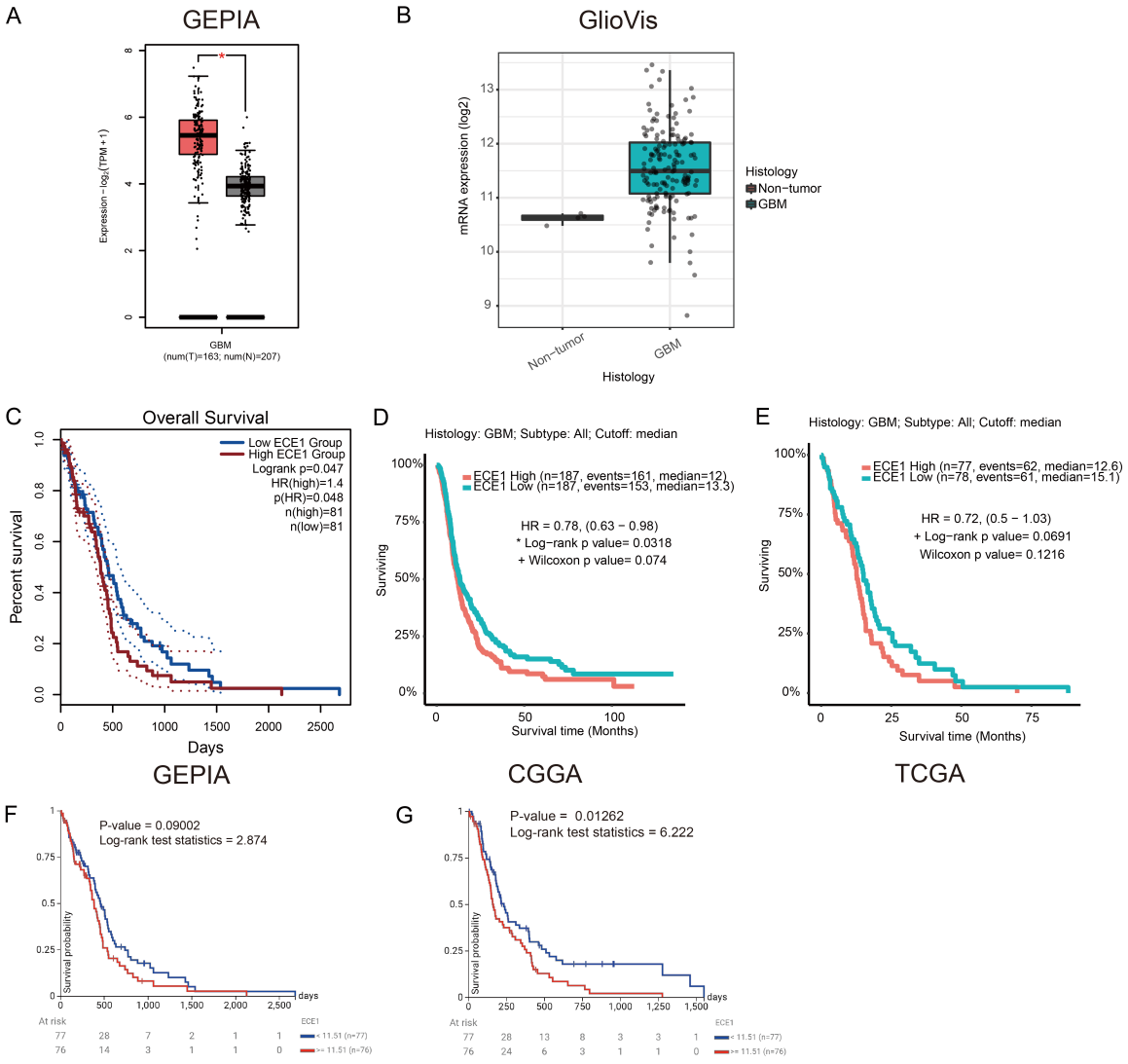

Figure S3. ECE1 expression correlates with GBM poor prognosis. (A, B) Expression levels of ECE1 in GBM and normal brain tissues were analyzed using the GEPIA and GlioVis platforms based on TCGA data. (C) Kaplan-Meier survival analysis demonstrating the association between ECE1 expression and overall survival in GBM patients using the GEPIA platform. (D, E) Validation of ECE1 expression and its prognostic relevance in CGGA and TCGA datasets using GlioVis. Although the Kaplan-Meier analysis in TCGA did not reach statistical significance when using the median cutoff (*P* = 0.0691), high ECE1 expression was significantly associated with poor survival in CGGA (*P* = 0.0318). (F, G) Analysis using the UCSC Xena platform (TCGA data; *P* = 0.09002, median cutoff) and progression-free interval as a clinical endpoint further supported the negative prognostic impact of ECE1 overexpression. Log-rank (C-G) were used for data analysis.

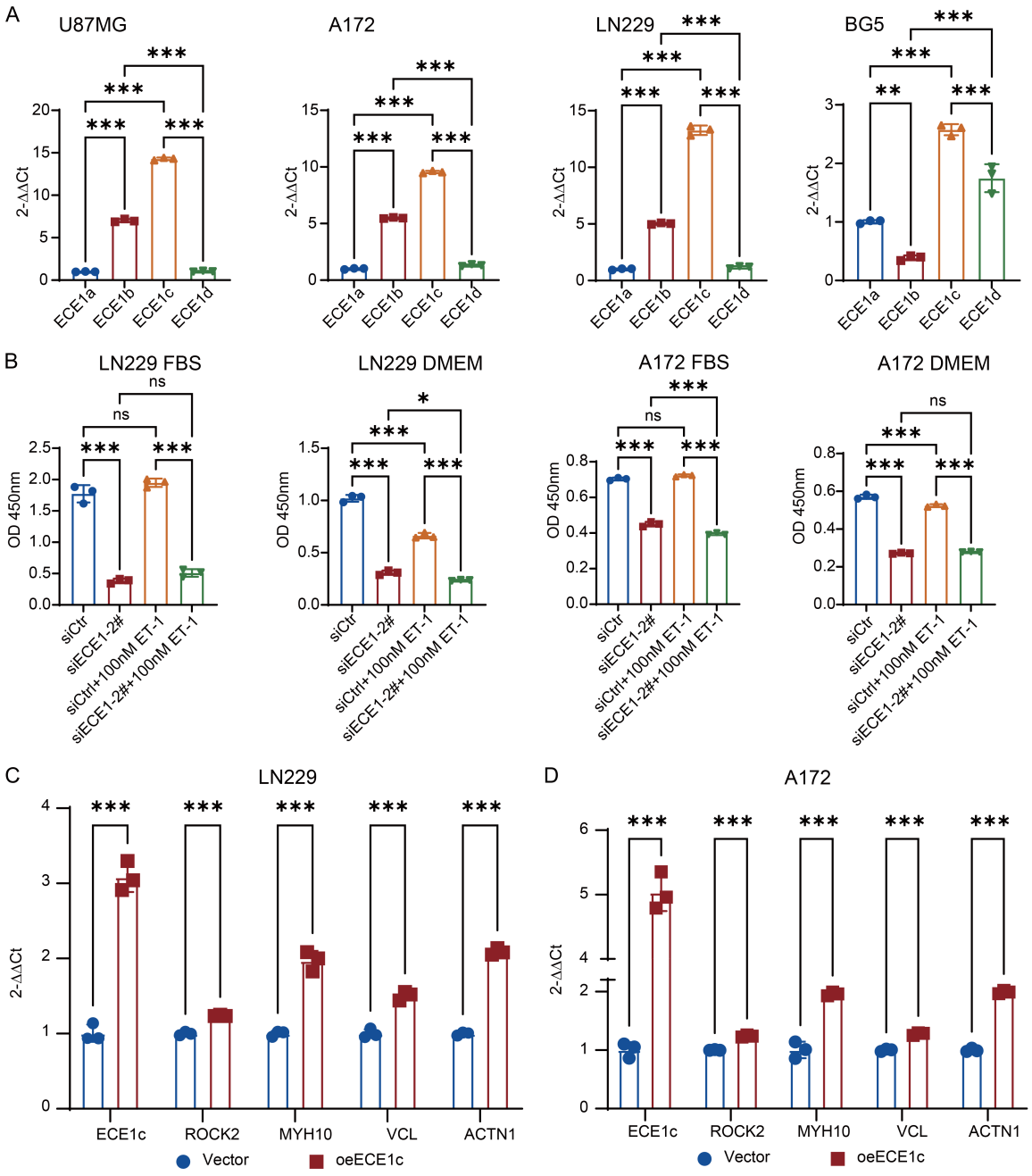

Figure S4. ECE1 isoform expression and the effect of ECE1c on cytoskeletal gene regulation. (A) qRT-PCR analysis of ECE1 isoforms (ECE1a-d) in GBM cell lines (U87MG, A172, LN229, and BG5) (n = 3 independent experiments). (B) Since endothelin-1 (ET-1) is rapidly degraded in medium containing fetal bovine serum (FBS), the rescue effect of exogenous ET-1 on ECE1 knockdown cells was evaluated under both serum-containing and serum-free DMEM conditions (n = 3 independent experiments). (C, D) qRT-PCR analysis of cytoskeleton-related genes (ROCK2, MYH10, VCL, and ACTN1) in LN229 and A172 cells overexpressing ECE1c, demonstrating activation of the actin cytoskeleton regulatory pathway upon ECE1c overexpression (n = 3 independent experiments). *ns* not significant, $*P < 0.05$, $**P < 0.01$, $***P < 0.001$; one-way ANOVA (A and B) and unpaired *t* test (C and D) were used for data analysis.

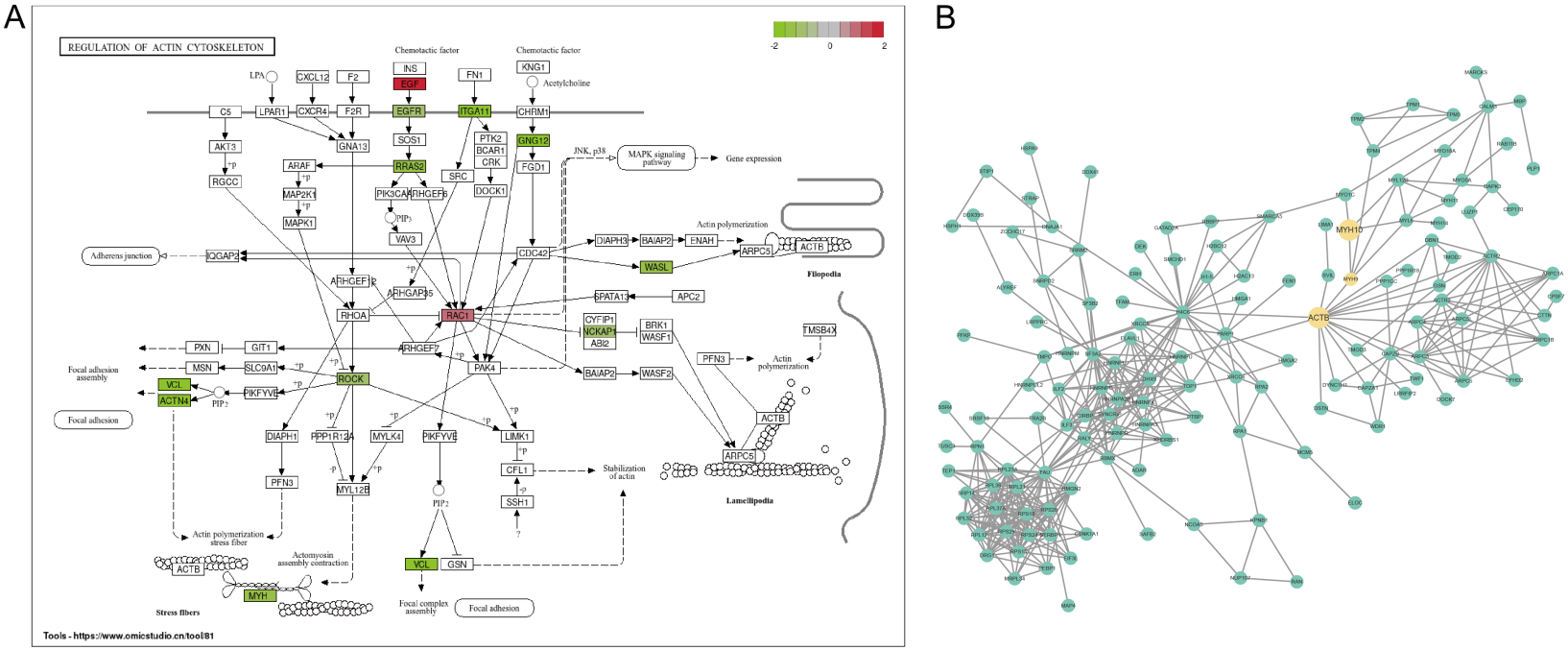

Figure S5. Actin cytoskeleton regulation pathway and ECE1 interacts with cytoskeletal proteins. A. Schematic representation of the actin cytoskeleton regulation pathway, with upregulated genes indicated in red and downregulated genes in green from RNA-sequencing. B. STRING-based protein-protein interaction (PPI) network constructed from mass spectrometry data identifying ACTB (β-actin) as an ECE1-interacting partner.